

1  
2  
3  
4  
5  
6  
7  
8  
9  
10  
11  
12  
13  
14  
15  
16  
17  
18  
19  
20  
21  
22  
23  
24  
25  
26  
27  
28  
29  
30  
31  
32  
33  
34  
35  
36  
37  
38  
39  
40  
41  
42  
43  
44  
45  
46  
47

**WORKING PAPER**  
**Uploaded to bioRxiv and SSRN**

**Single-dimensional human brain signals for two-dimensional economic choice options**

**Leo Chi U Seak\*, Konstantin Volkmann\*, Alexandre Pastor-Bernier, Fabian Grabenhorst and  
Wolfram Schultz**

\* These authors contributed equally to the study.

Department of Physiology  
Development and Neuroscience  
University of Cambridge  
Cambridge CB2 3DY  
United Kingdom

**Corresponding author:**

Wolfram Schultz  
Department of Physiology, Development and Neuroscience  
University of Cambridge  
Cambridge CB2 3DY  
United Kingdom  
Email: Wolfram.Schultz@Protonmail.com

**Email addresses of all authors:**

Leo Chi U Seak: chiuseak@gmail.com  
Konstantin Volkmann: konstantin.volkmann@googlemail.com  
Alexandre Pastor-Bernier: pastor-bernier@gmail.com  
Fabian Grabenhorst: fabian.grabenhorst@googlemail.com  
Wolfram Schultz: Wolfram.Schultz@protonmail.com

**Abbreviated title:** Neural processing of two-component choice options

**Number of pages:** 31

**Number of figures:** 4 (+ 5 supplementary figs), **tables:** 3 (+ 2 supplementary tables)

**Number of words:** Abstract: 189, Introduction: 650, Discussion: 1,496

**Conflict of interest:** The authors declare no conflicts of interest.

**Acknowledgements:** We thank Charles R. Plott for discussions and conceptual support, Steve Edgley for help and logistic support, Simone Ferrari-Toniolo for comments on experimental economics, Jae-Chang Kim and Putu Agus Khorisantono for suggestions on fMRI analysis, and Arkadiusz Stasiak for computer support. The Wellcome Trust supported this work (WT 095495, WT 204811).

**Abstract**

48  
49  
50 Rewarding choice options typically contain multiple components, but neural signals in single brain  
51 voxels are scalar and primarily vary up or down. In a previous study, we had designed reward  
52 bundles that contained the same two milkshakes with independently set amounts; we had used  
53 psychophysics and rigorous economic concepts to estimate two-dimensional choice indifference  
54 curves (IC) that represented revealed stochastic preferences for these bundles in a systematic,  
55 integrated manner. All bundles on the same ICs were equally revealed preferred (and thus had same  
56 utility, as inferred from choice indifference); bundles on higher ICs (higher utility) were preferred  
57 to bundles on lower ICs (lower utility). In the current study, we used the established behavior for  
58 testing with functional magnetic resonance imaging (fMRI). We now demonstrate neural responses  
59 in reward-related brain structures of human female and male participants, including striatum,  
60 midbrain and medial orbitofrontal cortex that followed the characteristic pattern of ICs: similar  
61 responses along ICs (same utility despite different bundle composition), but monotonic change  
62 across ICs (different utility). Thus, these brain structures integrated multiple reward components  
63 into a scalar signal, well beyond the known subjective value coding of single-component rewards.  
64

65

66

67

**Significance Statement**

68

69 Rewards have several components, like the taste and size of an apple, but it is unclear how each  
70 component contributes to the overall value of the reward. While choice indifference curves of  
71 economic theory provide behavioural approaches to this question, it is unclear whether brain  
72 responses capture the preference and utility integrated from multiple components. We report  
73 activations in striatum, midbrain and orbitofrontal cortex that follow choice indifference curves  
74 representing behavioral preferences over and above variations of individual reward components. In  
75 addition, the concept-driven approach encourages future studies on natural, multi-component  
76 rewards that are prone to irrational choice of normal and brain-damaged individuals.  
77

78

79 **Introduction**

80

81 In daily life, we choose between options that have multiple components. In a restaurant, we can get,  
 82 for the same price, a small but tasty steak or a larger but less tasty steak. In choosing the latter, we  
 83 give up some taste for more meat. Or the components can be distinct objects, like a meal with small  
 84 lasagne and big salad, or a meal with large lasagne and small salad; in choosing the latter, we give  
 85 up some salad for more lasagne. In both cases, our preference for an option (steak or meal) is based  
 86 on more than one component. To understand such choices, we need to know whether the value  
 87 integrated from different components can be represented by scalar measures of preferences and their  
 88 neuronal processes.

89 Functional magnetic resonance imaging (fMRI) studies investigated choices between bundles  
 90 with multiple-components. Several brain regions are involved in such choices, including striatum  
 91 (Hunt et al. 2014), frontal cortex (Hunt et al. 2014; Kurtz-David et al. 2019; Busemeyer et al. 2019),  
 92 cingulate cortex (Kurtz-David et al. 2019; Busemeyer et al. 2019; Fujiwara et al., 2009) and insula  
 93 (Busemeyer et al. 2019). One study showed encoding of values of gift cards that contained an  
 94 amount component and a quality component (de Berker et al. 2019); other studies investigated  
 95 irrational choices with monetary-gamble components (Kurtz-David et al. 2019) and addressed  
 96 irrational attraction and decoy effects (Chau et al. 2014; Gluth et al. 2017; Chung et al. 2017).  
 97 Whereas these studies demonstrated neural signals for multi-component rewards, they did not  
 98 specifically investigate whether the signals captured the reward value integrated from multi-  
 99 dimensional vectorial choice options. To resolve the issue would require to study how the increase  
 100 of one component compensates for the decrease of the other component without changing the  
 101 preference, and how such a trade-off is represented in scalar neural signals.

102 This trade-off mechanism constitutes the heart of indifference curves (IC) underlying  
 103 Revealed Preference Theory (Samuelson 1938). Each two-component choice option is graphically  
 104 represented at a specific x-y coordinate of a two-dimensional plot (Mas-Colell et al. 1995). All  
 105 bundles that are equally preferred to each other (choice indifferent, indicating same utility despite  
 106 different bundle composition) are located on the same IC irrespective of underlying variation in  
 107 bundle composition. Preferred bundles are located on higher ICs (farther away from the origin,  
 108 higher utility). This scheme is widely used for conceptualizing economic preferences in economics  
 109 textbooks, consumer choice (Simonson 1989; Tversky & Simonson 1993; Rieskamp et al. 2006),  
 110 animal choice (Kagel et al. 1975; Pastor-Bernier et al. 2017) and neuronal reward signals in animals  
 111 (Pastor-Bernier et al. 2019). The preference scheme has been extended to stochastic choice  
 112 (McFadden & Richter 1990; McFadden 2004), which is helpful for multi-trial statistical analyses of  
 113 human brain responses. Thus, the question for the current study arises: would human blood-oxygen-  
 114 level-dependent (BOLD) signals follow the characteristics of ICs that define the emergence of  
 115 scalar measures from vectorial bundles?

116 We investigated scalar BOLD signals for two-component milkshakes with sugar and fat  
 117 components that elicit subjective valuations and neural reward signals (Grabenhorst et al. 2010;  
 118 Zangemeister et al., 2016). We used three revealed preference levels (three ICs, different utility),  
 119 each estimated from five equally preferred bundles (indifference points, IPs, located on same IC,  
 120 same utility despite different bundle composition). Participants were presented with choice options  
 121 that contained one fatty and one sugary milkshake with specific amounts. We estimated  
 122 psychophysical indifference points (IP) at which a Reference bundle and a Variable bundle were  
 123 chosen with equal probability. From these IPs, we estimated well-ordered and non-overlapping ICs.  
 124 Using two independent general linear models, we found that scalar BOLD responses in striatum,  
 125 midbrain and medial orbitofrontal cortex followed the IC scheme: the responses varied  
 126 monotonically across ICs but changed only significantly along individual ICs, indicating orderly  
 127 integration of multi-component choice options into single-dimensional measures. The behavioral  
 128 results of this study have been published in detail (Pastor-Bernier et al. 2020).

129

## 130 **Materials and Methods**

131

### 132 **Participants**

133 A total of 24 participants (19–36 years old with mean age 25.4 years; 11 males, 13 females)  
134 performed a binary choice task that was followed, in 50% of trials, by a Becker–DeGroot–Marschak  
135 (BDM) task inside the fMRI scanner using sugary and fatty milkshakes. All participants had known  
136 milkshake appetite, and none had diabetes or lactose intolerance. All participants provided written  
137 consent based on an information sheet. The Cambridgeshire Health Authority (Local Research  
138 Ethics Committee) approved this study. The behavioral results have been published with more  
139 details separately (Pastor-Bernier et al. 2020).

140

### 141 **Experimental design**

142 The fundamental notion underlying this experiment posits that choice options consist of at least two  
143 components, and that preferences are revealed by observable choice. The multi-component choice  
144 options are called bundles. It is immaterial for the general concept of multi-component choice  
145 whether the individual components are parts of a single object (like size and taste of a steak in the  
146 example above) or constitute separate objects within a choice option (like lasagne and salad).  
147 Decision makers prefer bundles with larger or better components to those with smaller or worse  
148 components. Importantly, however, their preferences concern all components and are not directed at  
149 a single component alone. This property is manifested when participants prefer bundles in which  
150 one of the components of the preferred bundle is smaller than the same component in the non-  
151 preferred bundle (and the other component is large enough to overcompensate). At one point,  
152 participants may express equal preference for bundles in which the lower amount of one component  
153 is fully compensated by the higher amount in the other component, leading to choice indifference.  
154 We repeatedly measured choices with two options, each of which contained two milkshake  
155 components; the milkshakes constituted rewards, as shown by the voluntary consumption in all  
156 participants.

### 157 *Stimuli and rewards*

158 In each of the two bundles, we used stimuli to show the two milkshake components and their  
159 payout amounts (Fig. 1A). In each bundle stimulus, there were two rectangles aligned vertically.  
160 Each bundle component was indicated by the color of each rectangle. We extensively piloted  
161 various liquidized foods and liquids, and we found that milkshakes with a controlled mixture of fat  
162 and sugar give the most reliable across-participant behavioral performance. The presently used  
163 milkshakes with sugar and fat components that were found in previous studies to elicit subjective  
164 valuations and activate neural reward structures (Grabenhorst et al. 2010; Zangemeister et al.,  
165 2016). We delivered the milkshakes separately with a 0.5 s interval (see below). As drinks  
166 consisting of only sugar or only fat were considered as too unnatural, we used a high-fat low-sugar  
167 milkshake (75% double cream and 25% whole milk, with no sugar) as component A (top, blue), and  
168 a high-sugar low-fat milkshake (skimmed milk with 10% sugar) as component B (bottom, red).  
169 Inside each rectangle, the vertical position of a bar indicated the component's physical amount  
170 (higher was more). We delivered the milkshakes to the participants using a custom-made silicone  
171 tubing syringe pump system (VWR International Ltd). The pump was approved for delivering  
172 foodstuffs and was controlled by a National Instruments device (NI-USB-6009) via the Data  
173 Acquisition Toolbox in Matlab. We displayed stimuli to participants and recorded behavioral  
174 choices using the Psychtoolbox in Matlab running on a Windows (Dell) computer (Pastor-Bernier et  
175 al. 2020).

176

### 177 *Binary choice task before fMRI scanning*

178 In the binary choice task, each participant revealed one's preference in repeated choices between  
 179 two bundle stimuli, each indicating the amounts of two milkshake components (Fig. 1A). The two  
 180 bundles (stimuli) appeared on a computer screen simultaneously in front of the participant. The left  
 181 and right positions of the bundles were fixed but pseudorandomly alternated. Each bundle stimulus  
 182 included the same two kinds of milkshakes with independent physical amounts. Both stimuli  
 183 appeared after a pseudorandomly varying interval (mean 0.5 s) after a central fixation cross. In each  
 184 trial, the participant chose between the two bundles by pressing a button once (on a computer  
 185 keyboard; left or right arrow corresponding to choosing left or right bundle). We defined reaction  
 186 time as the interval between appearance of the two bundle stimuli and the participant's button press.  
 187 We delivered the two milkshakes to the participant from the chosen bundle with a probability  $P =$   
 188 0.2 using a Poisson distribution; i. e. the milkshake combination of one out of an average of five  
 189 chosen bundles was delivered, and no milkshake was delivered in the remaining trials. Component  
 190 B (high-sugar low-fat milkshake) was delivered at a constant interval of 0.5 s after component A  
 191 (high-fat low-sugar milkshake). We used this constant delay, instead of simultaneous delivery of  
 192 two milkshakes or a pseudo-randomly alternating milkshake sequence, to prevent uncontrolled  
 193 milkshake interactions, to maintain distinguishability of the individual milkshake rewards and to  
 194 keep temporal discounting constant. Therefore, the utility of component B derived from both  
 195 milkshake rewards and the temporal discounting specific for each milkshake. While the interval of  
 196 0.5 s was sufficiently short to not disrupt task performance and data collection, it was too short to  
 197 completely prevent the high-fat milkshake blending into the subsequent high-sugar milkshake  
 198 inside the participant's mouth. As the interval was kept constant in all participants and at all times,  
 199 the mixture provided a constant gustatory experience. Participants were asked not to eat or drink  
 200 anything at least four hours before the task performance. However, satiety may still be a concern  
 201 given the high fat and sugar content of our milkshakes. To address this issue, we set the probability  
 202 of  $P = 0.2$  payout schedule, limited each payout to 10.0 ml at most, and delivered no more than a  
 203 total of 200 ml of liquid to the participant in a session. We addressed the issue with additional  
 204 analyses and failed to find differential, sensory-specific satiety noticeable in choice probability  
 205 measures (see below; Pastor-Bernier et al. 2020).  
 206

### 207 *Psychophysical assessment of indifference points (IPs)*

208 We used a psychophysical staircase method (Pastor-Bernier et al. 2020; Green, & Swets, 1966) to  
 209 estimate the indifference points (IPs) at which, by definition, each of the two bundle options was  
 210 chosen equally frequently (i.e. probability  $P = 0.5$  for each option), indicating choice indifference  
 211 for the options. We established bundles at 15 IPs for each participant and used them in the  
 212 subsequent fMRI experiment.

213 To start the psychophysical procedure, we first set component A to 0 ml and component B to  
 214 either 2 ml, 5 ml or 8 ml in the Reference Bundle. We then systematically varied the Variable  
 215 Bundle. In the Variable Bundle, we first set the amount of its component A to one unit higher  
 216 (mostly 0.5 ml, 1.0 ml or 2.0 ml); we thereby specified the amount of component A gained by each  
 217 participant from the choice. We then randomly selected (without replacement) one amount of  
 218 component B from a total of seven fixed amounts (multiples of 0.5 ml), which span the whole,  
 219 constant range of amounts being tested. We repeatedly selected the amounts until we tested each of  
 220 the seven amounts once. We repeated estimation for each IP six times using a sigmoid function (see  
 221 Eqs. 1, 1a below), requiring a total of 42 choices for estimating each IP. The amount of component  
 222 B in the Variable Bundle was usually lower than the one in the Reference Bundle at the IP. With  
 223 these procedures, we assessed how much of component B a participant was willing to trade-in for  
 224 an additional unit of component A.

225 We obtained more IPs from the participants' choices between the fixed Reference Bundle and  
 226 the Variable Bundle, in which the amount of component A was increased stepwise, at each step  
 227 varying the amount of component B to estimate the choice indifference point at which the animal  
 228 was indifferent between the two bundles. Thus, bundle position advanced from top left to bottom  
 229 right on the two-dimensional IC (Fig. 1B). We are aware that testing with unidirectional progression

230 may cause particular variations in IP estimations than testing in a random sequence or in opposite  
 231 directions (Knetsch, 1989). However, our primary interest in this study was to investigate basic  
 232 neural processes in close relation to unequivocally estimated IPs and ICs rather than addressing the  
 233 more advanced features of irreversibility or hysteresis in ICs.

234 We used three different fixed amounts of component B for the Reference Bundle (2 ml, 5 ml,  
 235 or 8 ml), to obtain three IC levels. We estimated four IPs, together with the fixed reference bundle  
 236 as an IP, at each of three indifference curves (ICs; i.e. revealed preference levels), resulting in 15  
 237 IPs, in a total of 504 choices (trials) among 84 different choice option sets in each participant (6  
 238 repetitions for 7 psychophysical amounts at each of the 12 IPs).

239

## 240 **Statistical analysis**

### 241 *Numeric estimation of indifference points*

242 We used a sigmoid fit to numerically estimate the choice IPs. The fit was obtained from the  
 243 systematically tested choices with a generalized linear regression. The generalized linear  
 244 regressions used the *glmfit* function in Matlab (Matlab version R2015b) with a binomial distributed  
 245 probit model, which is an inversed cumulative distribution function (G). More specifically, we  
 246 apply the link function to the generalized linear regression  $y = \beta_0 + \beta_1 B_{\text{var}} + \varepsilon$  and write it as:

247

$$248 \quad G(y) = \beta_0 + \beta_1 B_{\text{var}} + \varepsilon \quad \text{Eq. 1}$$

249

250 where  $y$  represents the number of trials the Variable Bundle is chosen in each block of a six-  
 251 repetition series,  $\beta_0$  represent the constant offset,  $\beta_1$  represent the regression slope coefficient,  $B_{\text{var}}$   
 252 represent the physical reward amount (ml) of component B in the Variable Bundle, and  $\varepsilon$  represent  
 253 the residual error. We used the probit model as it assumes a multivariate normal distribution of the  
 254 random errors, which makes the model attractive because the normal distribution gives a good  
 255 approximation to most of the variables. The model does not hypothesize error independence and is  
 256 frequently used in econometrics (Razzaghi, 2013). On the other hand, the logit model, which is also  
 257 commonly used in economics, is simpler to compute but has more restrictive hypotheses on error  
 258 independence. Our preliminary data had shown a similar fit for both the logit and probit model,  
 259 therefore, we used the probit model fit because of its less restrictive hypotheses. Thus, we  
 260 approximated the IPs with the probit-model sigmoid fit, which can be written as follows:

261

$$262 \quad \text{Indifference Point} = -(\beta_0 / \beta_1) \quad \text{Eq. 1a}$$

263

264 where  $\beta_0$  and  $\beta_1$  represent coefficients of the generalized linear regression (Eq. 1). We obtained  
 265 these coefficients from the probit analysis (Amemiya, 1981).

266

### 267 *Indifference curves (ICs)*

268 In each participant, we obtained each single IC separately from an individual set of five equally  
 269 revealed preferred IPs with differently composed bundles using a weighted least-square non-linear  
 270 regression. We used a weighted regression to account for choice variability within participant; the  
 271 weight was defined as the inverse of the standard deviation of the titrated physical amount of  
 272 component B at the corresponding IP (the IP having been estimated with the probit regression). We  
 273 estimated the best  $\beta$  coefficients from the least-square regression to obtain a single IC (utility level),  
 274 using the basic hyperbolic equation:

275

$$276 \quad IC = \beta_0 + \beta_1 B + \beta_2 A + \beta_3 BA + \varepsilon \quad \text{Eq. 2}$$

277

278 where A and B represent physical amounts of component A and component B (ml), which refer to  
 279 the x and y axis, respectively. Note that  $(\beta_2 / \beta_1)$  is the slope coefficient and  $\beta_3$  is the curvature  
 280 coefficient of the non-linear least-square regression. As IC is a constant (representing one utility  
 281 level), we merged the IC constant with the offset constant ( $\beta_0$ ) and the error constant ( $\varepsilon$ ) into a

282 common constant  $k$ . To draw the ICs, we calculated the amount of component B from the derived  
 283 equation as a function of the amount of component A:

$$284 \quad B = (k - \beta_2 A) / (\beta_1 + \beta_3 A) \quad \text{Eq. 2a}$$

286 We graphically displayed the fitted ICs (Fig. 1B, C) by plotting the pre-set physical amount of  
 287 component A as the x coordinates, and calculated the fitted amount of component B, based on Eq.  
 288 2a, as the y coordinates. We estimated the error of the hyperbolic fit as the 95% confidence interval.  
 289 When calculating the ICs, we gave less weight to the IP with higher error. This model offered good  
 290 fits in our earlier work (Pastor-Bernier, et al. 2017; 2019; 2020). In this way, five IPs aligned to a  
 291 single fitted IC. For each participant, we fitted three ICs representing increasing revealed preference  
 292 levels (low, medium, high) farther away from the origin (Fig. 1B, C). The indifference map that  
 293 resulted from the 3 x 5 IPs was unique for each of the 24 participants. The indifference maps of the  
 294 24 participants were presented before (Pastor-Bernier et al. 2020).  
 295

#### 296 *Leave-one-out validation of ICs*

297 We used a leave-one-out analysis to test the validity of the hyperbolic IC fit to the IPs. We  
 298 systemically removed one IP in each IC (excluding the initial Reference Bundle at  $x = 0$ ), and then  
 299 fitted the IC again using the hyperbolic model. We then assessed the differences (deviation)  
 300 between the original IC (without IP removal) and the new IC without the one left-out IP. The  
 301 deviation was defined as the Euclidean distance of component B between the original (left-out) IP  
 302 and the IP estimated from the refitted IC:  
 303

$$304 \quad d = B_{IP} - B_{refit} \quad \text{Eq. 3}$$

305 with  $d$  representing the difference (i.e. residual; in ml; y-axis),  $B_{IP}$  representing the physical amount  
 306 of component B in the left-out IP (ml), and  $B_{refit}$  representing the estimated physical amount of  
 307 component B in the refitted IC (ml). In this way a residual of 0 ml suggested that removal of the  
 308 left-out IP did not change the shape of that IC, while any residual unequal to 0 ml could quantify the  
 309 deviation.  
 310  
 311

#### 312 *Control of alternative choice factors*

313 To assess the potential influence of other factors affecting the participants' choice, we performed a  
 314 logistic regression fit on choices to test whether the choices were indeed explained by the bundle  
 315 components. We performed a random-effect logistic regression on the choice data from each  
 316 participant as follows:  
 317

$$318 \quad y = \beta_0 + \beta_1 \text{RefB} + \beta_2 \text{VarA} + \beta_3 \text{VarB} + \beta_4 \text{RT} + \beta_5 \text{VarPos} + \beta_6 \text{PChoice} + \varepsilon \quad \text{Eq. 4}$$

319 with  $y$  as a dummy variable (either 1 or 0, indicating choosing or not choosing the Variable Bundle),  
 320 RefB as physical amount (ml) of component B in the Reference Bundle, VarA and VarB as physical  
 321 amount (ml) of components A and B in the Variable Bundle, RT as reaction time (ms), VarPos  
 322 indicating left or right position (0 or 1) of the Variable Bundle stimuli shown on the computer  
 323 screen relative to the Reference Bundle, and PChoice representing choice of the previous trial (0 or  
 324 1). Each  $\beta$  coefficient was normalized by multiplying the standard deviation of the respective  
 325 independent variable and dividing by the standard deviation of the dependent variable ( $y$ ). We  
 326 subsequently used a one-sample t-test against 0 to assess the statistical significance of each of the  
 327 beta ( $\beta$ ) coefficients.  
 328

329 We assessed the normalized beta ( $\beta$ ) coefficients and p-values for each individual participant  
 330 and then calculated averages across 24 participants. With the regression model, we found a negative  
 331 correlation of choosing the Variable Bundle and the amount of component B in the Reference  
 332 Bundle (RefB:  $\beta = -0.43 \pm 0.16$ ,  $P = 0.020 \pm 0.005$ ; mean  $\pm$  SEM) (amount of component A in the  
 333

334 Reference Bundle was always a constant 0 ml). We also found positive correlation of choosing the  
 335 Variable Bundle and amount of both component A and component B in the Variable Bundle (VarA:  
 336  $\beta = 0.67 \pm 0.16$ ,  $P = 0.009 \pm 0.004$ ; VarB:  $\beta = 0.94 \pm 0.33$ ,  $P = 0.012 \pm 0.009$ ). We further found  
 337 that for these three variables, the beta ( $\beta$ ) coefficients significantly differed from 0 with one-sample  
 338 t-tests ( $P = 0.012$ ,  $P = 0.00088$  and  $P = 0.00028$ , respectively), confirming the robustness of these  
 339  $\beta$ . Thus, we confirmed that the choices depended on the amount of reward of both Variable and  
 340 Reference Bundle. We also validated that both bundle components were important for the choices.  
 341 All remaining variables in the regression, including reaction time, left or right position of the  
 342 Reference Bundle on the computer screen and choice of the previous trial, failed to account  
 343 significantly for the participant's current choice ( $P = 0.754 - 0.988 \pm 0.003 - 0.290$ ). We therefore  
 344 conclude that, in our experiment, the bundles with their two components, instead of other factors,  
 345 account for the revealed preference relationships.

#### 346 *Satiety control*

347 Besides considering other components in the design, we also tested potential effects of satiety.  
 348 Satiety may have affected the preferences for the two bundle components, even if the rewards were  
 349 paid out only in one fifth of the trials on average and were limited to less than 200 ml. Differences  
 350 in devaluation between the two component milkshake might be a major factor for changing in an  
 351 uncontrolled manner the currency relationship of the two components. This kind of unequal  
 352 devaluation should result in a graded change in the instantaneous choice probability around the IPs  
 353 over the test steps of 42 trials. We used the following equation to calculate the instantaneous choice  
 354 probability:

$$355 \quad y = \sum_{(n=1 \text{ to } 6)} (CV / TS) \quad \text{Eq. 5}$$

356 with  $y$  representing the instantaneous probability ( $P$  ranging from 0.0 to 1.0), CV represent choice  
 357 or not-choice of Variable Bundle (1 or 0), and TS represent test step (repetition 1-6).

358 We found only insignificant fluctuations in choice probabilities, without any consistent  
 359 upward or downward trend in the 1-way repeated measures ANOVA, together with the post-hoc  
 360 Tukey Test (above IP:  $F(5, 41) = 0.28$ ,  $P > 0.05$ ; below IP:  $F(5, 41) = 1.53$ ,  $P > 0.05$ ).

#### 361 **Behavioral task during fMRI scanning**

362 During scanning, we used a value elicitation task that allowed more trials in a shorter time frame. At  
 363 the beginning of each trial, one bundle was shown to the participant for 5 s (bundle-on phase in Fig.  
 364 1E) in the center of the computer monitor after the initial fixation period (500 ms). The bundle was  
 365 pseudorandomly selected from the 15 IP bundles in three ICs of each participant. Bundle  
 366 composition (amounts of the two components) was set in each participant according to performance  
 367 in the binary choice task before fMRI scanning. Hence, the 15 bundles for each participant were not  
 368 identical across participants. Subsequently, a fixation cross appeared for a pseudorandomly varying  
 369 interval (mean 2s). In 50% of the trials (pseudorandomly selected), the task was terminated after  
 370 this fixation cross.

371 In the other 50% of the trials, we presented the participant with a Becker-DeGroot-Marschak  
 372 (BDM) task that was akin to a second price auction (Becker, DeGroot, & Marschak, 1964). This  
 373 task served as an independent mechanism that related the estimated ICs to stated utility. In the BDM  
 374 (bidding phase in Fig. 1E), we gave the participant a fresh 20 UK pence endowment on each trial.  
 375 Using this endowment, the participant bid for a two-component bundle against a pseudorandom  
 376 computer bid (extracted from a normal distribution with replacement). To bid, the participant moved  
 377 a cursor, shown on the computer screen, horizontally with the left and right keyboard arrows. We  
 378 registered the BDM bid (position of the cursor) 5 s after presenting the bidding scale to the  
 379 participant. When bidding no less than the computer, the participant received the bundle  
 380 (milkshake) reward from both components and paid the monetary value equal to the computer bid.  
 381 By contrast, when bidding less than the computer, the participant lost the auction, paid nothing and



386 would not get any bundle (milkshake) reward. We showed the participant the result of the auction  
 387 immediately after having placed the bid, by displaying a respective win (green circle) or loss (red  
 388 square) stimulus on the computer monitor (Fig. 1E); when winning the bid, the participant received  
 389 the milkshake rewards in the sequence and frequency as in the binary choice task.

390 We first selected one bundle randomly (without replacement) from the participant-specific set  
 391 of 15 bundles (the 15 bundle IPs used to fit the 3 ICs as shown in Fig. 1). Then we showed the  
 392 participant the selected single bundle during the bundle-on phase. We presented each of the 15  
 393 bundles to the participant for 24 times, resulting in a total of 360 trials, which included 180 trials  
 394 (50%) with BDM bidding (Fig. 1E), and we used the average of these bids as the participant's  
 395 BDM-estimated utility.

396 First, we assessed whether the BDM bids increased for bundles across revealed preference  
 397 levels but were similar for IP bundles on the same revealed preference level, using Spearman rank  
 398 correlation analysis and further confirmation with the Wilcoxon signed-rank test (note that this  
 399 analysis used the coordinates of the individual IPs to which the ICs had been fitted, not the IC  
 400 coordinates themselves). We also performed a generalized linear regression with a Gaussian link  
 401 function (random-effect analysis) for each participant and then averaged the  $\beta$  coefficients and p-  
 402 values across all participants. We used the following generalized linear regression:

$$403 \quad y = \beta_0 + \beta_1 \text{ PrefLev} + \beta_2 \text{ AmBundle} + \beta_3 \text{ TrialN} + \beta_4 \text{ PrevBid} + \beta_5 \text{ Consum} + \varepsilon \quad \text{Eq. 6}$$

404 with  $y$  representing amount of monetary bid, PrefLev representing revealed preference level (low,  
 405 medium, high), AmBundle representing the summed amount (ml) of component A and component  
 406 B in the currency of component A (converted with Eq. 2a), TrialN representing trial number,  
 407 PrevBid representing amount of monetary bid in the previous trial, and Consum representing  
 408 accumulated consumption amount (ml) of component A and component B until that point in the  
 409 experiment. We normalized each  $\beta$  coefficient by multiplying the standard deviation of the  
 410 respective independent variable, and then dividing by the standard deviation of the dependent  
 411 variable  $y$ . We performed a subsequent one-sample t-test against 0 to assess the significance of each  
 412 beta ( $\beta$ ) coefficient across all 24 participants. We found significant beta ( $\beta$ ) coefficients of BDM  
 413 monetary bids to the preference level (PrefLev:  $\beta$ -coefficient difference from 0:  $P = 0.000026$  with  
 414 one-sample t-test; mean across all 24 participants:  $\beta = 0.47 \pm 0.09$ ,  $P = 0.016 \pm 0.015$ ; mean  $\pm$  SEM)  
 415 and bundle amount (AmBundle:  $P = 0.0278$ ;  $\beta = 0.15 \pm 0.13$ ;  $P = 0.020 \pm 0.017$ ), but not in trial  
 416 number (TrialN:  $\beta = -0.10 \pm 0.25$ ;  $P = 0.726 \pm 0.354$ ), previous trial bid (PrevBid:  $\beta = 0.12 \pm 0.11$ ;  $P$   
 417  $= 0.676 \pm 0.427$ ) nor consumption history (Consum:  $\beta = 0.12 \pm 0.11$ ;  $P = 0.224 \pm 0.185$ ).

#### 421 **fMRI data acquisition**

422 The functional neuroimaging data in this study were collected using a 3T Siemens Magnetom Skyra  
 423 Scanner at the Wolfson Brain Imaging Centre, Cambridge, UK. Echo-planar images (T2-weighted)  
 424 with blood-oxygen-level-dependent (BOLD) contrast were acquired at 3 Tesla across two days with  
 425 each participant. All images were in plane resolution  $3 \times 3 \times 2$  mm, 56 slices were acquired with 2  
 426 mm slice thickness, repetition time (TR) = 3 s, echo time (TE) = 30 ms, -90 deg flip angle and -192  
 427 mm field of view. To reduce signal dropout in medial-temporal and inferior-frontal regions during  
 428 the scanning, the acquisition plane was tilted by -30 degrees and the z-shim gradient pre-pulse was  
 429 implemented. We also applied MPRAGE sequences and co-registered to acquired high-resolution  
 430 T1 structural scans for group-level anatomical localization with  $1 \times 1 \times 1$  mm<sup>3</sup> voxel resolution,  
 431 slice thickness of 1 mm, 2.3 s TR, 2.98 ms TE, 9 deg flip angle and 900 ms inversion time.

#### 433 **fMRI data analysis**

434 We used the Statistical Parametric Mapping package to analyze the neuroimaging data (SPM 12;  
 435 Wellcome Trust Centre for Neuroimaging, London). We pre-processed the data by realigning the  
 436 functional data to include motion correction, normalizing to the standard Montreal Neurological  
 437 Institute (MNI) coordinate, and then smoothing using a Gaussian kernel with the full width at half

438 maximum (FWHM) of 6 mm within data collected on the same day. We then segmented the data to  
 439 extract white matter, grey matter and cerebrospinal fluid (CSF) and followed by co-registering the  
 440 two-day data using the T1-weighted structural scans from each day. We then applied a high-pass  
 441 temporal filter to it with a 128 s cut-off period. We applied General linear models (GLMs), which  
 442 assumed first-order autoregressions, to the time course of activation. We modeled event onsets, in  
 443 the time course of activation, as single impulse response functions convolved with the canonical  
 444 hemodynamic response. We included the time derivatives in the functions set and defined linear  
 445 contrasts of parameter estimates to test the specific effect in each participant's dataset. We obtained  
 446 voxel values for each contrast in the format of a statistical parametric map with corresponding t-  
 447 statistic. We applied a standard explicit mask (mask\_ICV.nii) at the first level analysis to mask out  
 448 all activations outside of the brain. To test our specific hypotheses, we used the following GLMs:  
 449

450 *General linear model 1 (GLM1)*

451 This GLM served to search for regions whose stimulus-induced brain activations varied across ICs  
 452 (high > low) but not along the same ICs in the bundle-stimulus-on phase (two-level t-test analysis,  
 453 Fig. 2). For each participant, we estimated a GLM with the following regressors (R) of interest:  
 454 (R1-R15) as indicator functions for each condition during the bundle-on phase (for the 15 different  
 455 bundles), at the time when participant was presented with the visual bundle cue representing the  
 456 milkshakes bundles; (R16) as indicator function for the BDM bid, at the time when the participant  
 457 made the bid; (R17) as R16 that was modulated by the response to the participant's bid (1 - 20);  
 458 (R18) as indicator function for the losing bid, at the time when the participant was presented with  
 459 visual cues showing the loss of bidding of the trial; (R19) as indicator function for the auction win  
 460 phase, at the time when the participant was presented with the visual cues representing the winning  
 461 of bidding; (R20) as indicator function for the reward phase, i.e. the times when participants  
 462 received the milkshakes; (R21) as R20 that was modulated by reward magnitude (in mL).  
 463 Regressors R16 - R19 were not used further for this analysis and served only to regress out potential  
 464 BDM effects in the 50% of trials that included BDM.

465 In the second (group random-effects) level analysis, we entered the all 24 participant-specific  
 466 linear contrasts of the first-level regressors R1-R15 (representing 5 bundles on each of the three  
 467 preference levels) into t-tests (high > low revealed preference level) using Flexible Factorial  
 468 Design, resulting in group-level statistical parametric maps. In the Flexible Factorial design matrix  
 469 (second-level analysis), the following second-level regressors were used: (R1-24) indicator  
 470 functions of participant's identifier representing participant 1 - 24 (within participant effect); (R25-  
 471 27) indicator functions of the three revealed preference levels (across ICs) (R28-32), indicator  
 472 functions of the 5 bundles representing amount of Component A in increasing magnitude or amount  
 473 of Component B in decreasing magnitude (along the same ICs). We first calculated the main  
 474 contrast image based on high>low revealed preference level (t-tests). Second, we calculated a mask  
 475 contrast based on 5 bundles of Component A in increasing magnitude (t-tests). Third, we calculated  
 476 another mask contrast based on 5 bundles of Component B in increasing magnitude (t-tests). The  
 477 final result of GLM1 was represented by the main contrast (high>low revealed preference level)  
 478 masking out (with exclusive mask) the two mask contrasts, controlling of the brain responses along  
 479 the same ICs.

480  
 481 *General linear model 2 (GLM2)*

482 This GLM identified regions associated with the binary comparisons of partial physical non-  
 483 dominance bundles (Fig. 3). The GLM searched for brain regions in which activations were higher  
 484 for bundles that were on a higher revealed preference level than bundles in which one component  
 485 was physically higher than in the preferred bundle (partial physical non-dominance). In the first-  
 486 level estimation, regressors were the same as in GLM1 with the 21 regressors described above. In  
 487 the second-level analysis, we entered all pairs of bundles that met the following criteria: (Bundle 1):  
 488 partial physical non-dominance bundles with higher revealed preference level, but less (with at least  
 489 0.2mL less in Components A or 0.4mL less in Component B) in one component; (Bundle 2): partial

490 physical dominance bundles with lower revealed preference level, but more in one component. A  
 491 third level group-level analysis (one-sample t-test) was performed with contrast images from the  
 492 second level to generate group-level statistical parametric maps across 24 participants.

493

#### 494 *General linear model 3 (GLM3)*

495 This GLM identified brain regions in which activity correlated with the amount of BDM bid (0 - 20  
 496 pence) during the bidding phase (Fig. 4B). In the first-level estimation, we used the following  
 497 regressors and parametric modulators: (R1) as indicator function of bundle-on phase; (R2) as R1  
 498 modulated by amount of BDM bid; (R3) as indicator function of BDM bidding phase (50% of  
 499 trials); (R4) as R3 modulated by amount of BDM bid; (R5) as indicator function of intertrial  
 500 interval when there was no bidding phase (50% of trials); (R6) as indicator function at onset of the  
 501 loss cue, when the participant lost the BDM bidding; (R7) as indicator function at onset of the win  
 502 cue, when the participant won the BDM bidding; (R8) as indicator function at onset of milkshake  
 503 delivery; (R9) as R8 modulated by physical amount of milkshake; (R10) as contrast of win cue  
 504 onset versus loss cue onset; (R11) as contrast of loss cue onset versus win cue onset. In the second-  
 505 level analysis, a one-sample t-test analysis was performed with contrast images from the first level  
 506 to generate group-level statistical parametric maps across 24 participants.

507

#### 508 *Small volume corrections*

509 To derive coordinates for small-volume correction in GLM1 and GLM2, we entered the term  
 510 “reward anticipation” in the Neurosynth meta-analysis database (Yarkoni et al., 2011) to obtain  
 511 MNI coordinates. The meta-analysis employed a total of 92 independent studies that showed  
 512 correlation of value elicitation with various brain regions. Our study used MNI coordinates of  
 513 ventral striatum [12, 10, -8], medial orbital frontal cortex (mid-OFC) [20, 46, -18] and midbrain [8,  
 514 -18, -14], obtained from this Neurosynth meta-analysis database. We used a sphere with 6 mm  
 515 radius for midbrain and striatum, and 10 mm for OFC, following the common approach of using 6  
 516 mm radius spheres for subcortical structures and larger spheres for cortical structures (Zangemeister  
 517 et al., 2016, De Martino et al., 2009, Chib et al., 2009).

518 We aimed at finding activity correlating with the BDM bid in GLM3. Therefore, for small  
 519 volume correction analysis in GLM3, we used a MNI coordinate of dorsal striatum [12, 14, 4]  
 520 found in a previous study with BDM bidding (De Martino et al., 2009). We did not use coordinates  
 521 from Neurosynth in GLM3 because datasets related to BDM or other auctions were not available in  
 522 the Neurosynth database.

523

#### 524 **Region-of-interest (ROI) analysis**

525 We selected significantly activated regions from brain maps established with GLM1, GLM2 or  
 526 GLM3 for further ROI analysis. We extracted raw BOLD data from ROI coordinates based on  
 527 group clusters, which we defined independently for each participant using a leave-one-out  
 528 procedure based on the result of GLM1, GLM2 or GLM3. In the leave-one-out procedure, we re-  
 529 estimated the second-level analysis 24 times, each time leaving out one participant, to define the  
 530 ROI coordinates for the left-out participant. Following data extraction, we applied a high-pass filter  
 531 with a cut off period of 128 s. The data was then z-normalized, oversampled by a factor of 10 using  
 532 the Whittaker–Shannon interpolation formula, and separated into trials to produce a matrix of trials  
 533 against time.

534 A total of 3 ROI analyses were performed in this study. First, a Spearman rank analysis was  
 535 used to examine BOLD signals that changed across ICs but not along ICs (corresponding to GLM1  
 536 and GLM3). Second, a bar chart was used to illustrate the three revealed preference levels in  
 537 different ROIs (corresponding to GLM1). Third, a bar chart was used to show activation changes  
 538 between bundles with partial physical non-dominance on different revealed preference levels  
 539 (corresponding to GLM2).

540

#### 541 *Spearman rank*

542 In the Spearman rank analysis, we first regressed out the motion parameters (artefact) from the  
 543 BOLD response with generalized linear models. Then we used the participant's residual BOLD  
 544 response to generate time courses of Spearman rank correlation (Rho) coefficients.

545 For GLM1, we tested the correlation between BOLD response (during the bundle-on phase)  
 546 and revealed preference level (across-IC analysis). We then calculated group averages and standard  
 547 errors of the mean for each time point for all participants, yielding averaged participant effect size  
 548 time courses (Fig. 2C). In the along-IC analysis, we ranked the bundles along the same IC with  
 549 individual participant's BOLD signal (Fig. 2D). A subsequent one-sample t-test against 0 served to  
 550 assess the significance of the Rho coefficients across subjects.

551 For GLM3, we tested the correlation of the BOLD response (BDM bidding phase) and the  
 552 amount of BDM bids. Similar to GLM1, we then calculated group averages and standard errors of  
 553 the mean of the Rho coefficients for each time point for all participants (Figs. 4B, 4-1). A  
 554 subsequent one-sample t-test against 0 served to assess coefficient significance.

555

#### 556 *Bar chart for revealed preference level analysis*

557 We used bars to illustrate how different IC levels were encoded in each region of the brain. To  
 558 generate an ROI bar chart, the BOLD response was first extracted using the leave-one-out  
 559 procedure described above. For each participant, we obtained three generalized linear model fits to  
 560 the BOLD signal at timepoint 6 s. In each generalized linear model fit, the identifier of one level of  
 561 revealed preference was entered as a regressor (dummy variable, e. g. 1 for bundles with high  
 562 preference level and 0 for middle or low preference level) together with motion parameter  
 563 regressors, which served to eliminate the motion artefact. We obtained beta ( $\beta$ ) coefficients of each  
 564 level of revealed preference from the fit and then calculated the mean and standard error of the beta  
 565 coefficient. We then plotted the bar charts shown in Fig. 2E. Paired t-tests were used to compare  
 566 beta coefficients between different revealed preference levels. As a control, we also obtained beta  
 567 ( $\beta$ ) coefficients of 5 indifference points from the same level of revealed preference, averaged across  
 568 the three levels, and then calculated the mean and standard error of the beta coefficient across  
 569 participants. We then plotted the bar charts shown in Fig. 2F. One-way ANOVAs were used to  
 570 compare beta coefficients between the 5 indifference points.

571

#### 572 *Bar chart for partial physical non-dominance analysis*

573 A bundle was defined as being partially physically non-dominant over another bundle if one of its  
 574 milkshake components had a physically lower amount than the same component in the dominated  
 575 bundle. Thus, the revealed preferred bundle was partially physically non-dominant. For an ROI  
 576 analysis of partial physical non-dominance, we fitted three generalized linear models to the BOLD  
 577 response with bundle identifiers, which were two dummy variables representing partially physically  
 578 dominance bundles (lower revealed preference despite larger physical amount in one milkshake)  
 579 and partial physical non-dominance bundles (higher revealed preference despite smaller physical  
 580 amount in one milkshake). Three generalized linear models were used to fit bundles in low vs.  
 581 middle, middle vs. high, and low vs. high comparisons, respectively. The domination was defined as  
 582 at least 0.2 ml more for component A or at least 0.4 ml more for component B, as in GLM2. We  
 583 calculated the mean and standard error of the averaged beta ( $\beta$ ) coefficients across participants at  
 584 time point 6 s and plotted the bar chart as shown in Fig. 3C. Paired t-tests were used to compare  
 585 beta coefficients between partial physical dominance bundles and partial physical non-dominance  
 586 bundles. Motion parameters were also used as regressors for each participant to eliminate motion  
 587 artefacts. In addition to extracting BOLD signal with leave-one-out peaks of GLM2 (Fig. 3C), we  
 588 also extracted BOLD signal with leave-one-out peak from GLM1 (Fig. 3-1) to confirm the  
 589 robustness of this analysis.

590

#### 591 **Reward prediction errors (RPE)**

592 The current task did not involve learning in which reward would occur in a partly unpredicted  
 593 manner and thus elicit RPEs. The only RPE could occur at the unpredicted time of the first stimulus

594 that explicitly and quantitatively predicted the reward amounts of the bundle components indicated  
 595 by the bundle stimulus. Conceivably, in the most simple form, the RPE would reflect the integrated  
 596 reward amounts of both bundle components relative to the prediction derived from the past trial  
 597 history. There were three levels of bundle stimulus corresponding to the three IC levels. Thus,  
 598 appearance of a given bundle stimulus would elicit an RPE relative to the past experienced bundles,  
 599 weighted by the learning coefficient. Thus, reward prediction errors would have values around -1, 0,  
 600 and +1 for bundles located on low, intermediate and high ICs, respectively, the variation depending  
 601 on the learning coefficient. For comparison, the bundle stimulus at each IC level without any RPE  
 602 would have values of 1, 2 and 3, respectively. Thus, neural responses to the RPE and to the stimulus  
 603 directly (i. e. without subtraction of prediction) would result in very similar regression slopes  
 604 (depending on the learning constant used for computing the RPE) and thus be difficult to  
 605 distinguish from each other. We modelled RPEs with various learning coefficients in the range  
 606 between 0.1 and 0.9 and for all values found high correlations between RPE and bundle stimulus  
 607 value at the three IC levels. For example, a learning coefficient of 0.2 in a Rescorla-Wagner model  
 608 resulted in a Spearman-rank correlation of  $0.9337 \pm 0.00085$  SEM ( $n=15$  bundles  $\times$  24 trials = 360  
 609 trials  $\times$  24 subjects pooled). For this reason, a RPE analysis would not yield new insights and will  
 610 not be further reported.

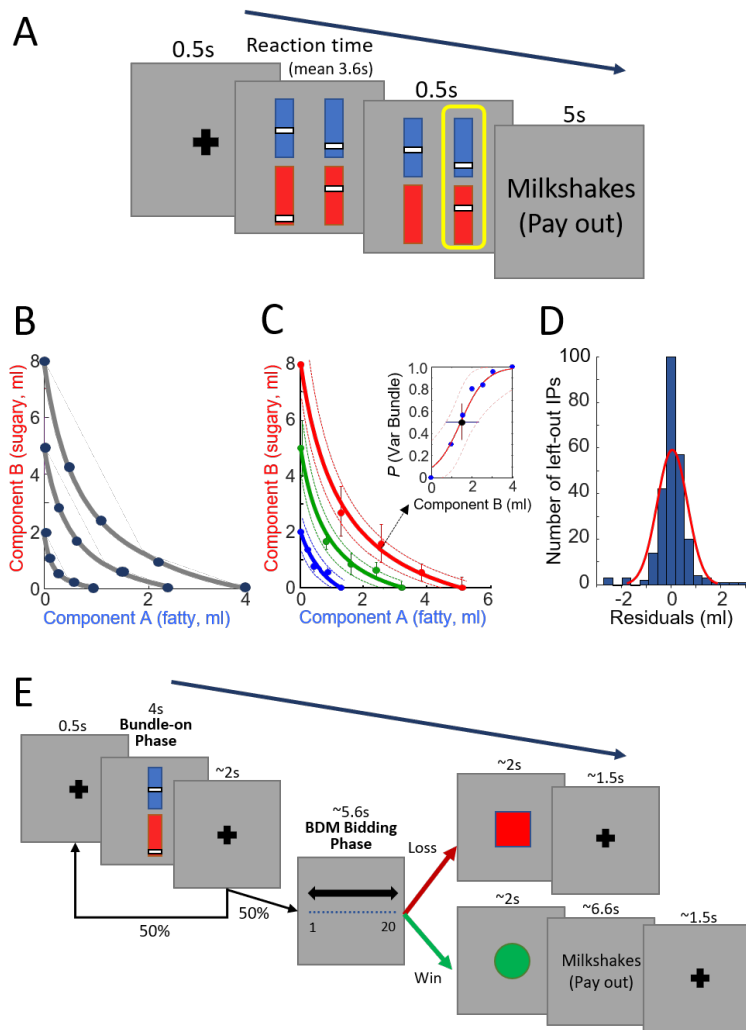
## 611 **Results**

### 612 **Implementation of indifference curves**

613  
 614 Participants ( $n = 24$ ) chose between two visual stimuli in repeated trials. Each of the two bundle  
 615 stimuli represented a two-component bundle that contained the same two milkshakes with  
 616 independently set amounts (Fig. 1A; see Methods). Thus, we implemented choices between bundles  
 617 with separate objects (two milkshakes) rather than choices between single objects that each had  
 618 multiple components. Each stimulus contained two colored vertical rectangles: the blue rectangle  
 619 represented component A (low-sugar high-fat milkshake); the red rectangle represented component  
 620 B (high-sugar low-fat milkshake). In each rectangle, a vertically positioned bar indicated the  
 621 physical amount of each component milkshake, where higher was more.

622 We examined choices between: (1) a pre-set Reference bundle and (2) a Variable bundle  
 623 whose component A had a fixed test amount and whose component B varied pseudorandomly. In all  
 624 24 participants, choice probabilities followed the component B monotonically. We obtained each  
 625 indifference point (IP; choice probability  $P = 0.5$  for each bundle, indicating equal preference and  
 626 same utility despite different bundle composition) from a set of six-repetition choices using a probit  
 627 choice function (Eqs. 1, 1a). We thereby obtained a two-dimensional IP that showed the amounts of  
 628 the two components of the Variable Bundle between which the participant was indifferent against  
 629 the constant Reference Bundle. We repeated this procedure, keeping the Reference Bundle constant  
 630 and increasing the amounts of component A in the Variable Bundle, thus obtaining a set of IPs. All  
 631 IPs in such a set were equally revealed preferred to, and thus had the same utility as, the constant  
 632 Reference Bundle.

633 In each participant, we estimated a total of three sets of IPs (each containing 5 IPs) by pre-  
 634 setting three different amounts of component B (2 ml, 5 ml or 8 ml with component A always 0 ml)  
 635 in the Reference Bundle. Each IP defined the trade-off between the two components; it indicated  
 636 how much of component B the participant was willing give up in order to gain one unit of  
 637 component A without change of preference. We derived each IC from such a set of five IPs by  
 638 hyperbolic fitting (Eqs. 2, 2a; Fig. 1B, C). Taken together, the IPs with the continuous ICs  
 639 represented revealed preferences in a systematic manner, thus implementing the basic concepts  
 640 underlying this study.  
 641  
 642



643  
644

**Figure 1.** Experimental procedure and behavior.

646 (A) Choice task outside the fMRI scanner. The participant chose between a reference bundle and a varied test bundle.  
647 Each bundle consisted of two components, Component A (blue bar) and Component B (red bar). The amount of each  
648 component was indicated to the participant by the height of a white bar (higher was more). Component A was a low-  
649 sugar, high-fat milkshake. Component B was a low-fat high-sugar milkshake. The two milkshakes of the chosen bundle  
650 were delivered at the end of each trial with a probability of  $P = 0.2$ .

651 (B) Schematic diagram of three indifference curves (ICs) and five indifference points (IPs) on each IC (same data points  
652 as shown in Fig. 1F of Pastor-Bernier et al. 2020).

653 (C) Example ICs from a typical participant. Solid lines represent three ICs (hyperbolically fitted by IPs). Dotted lines  
654 represent 95% confidence interval of the hyperbolic fit. The inset shows the psychophysical function of one IP. The IP  
655 (black dot in the inset) was estimated by probit regression on the test points (blue dot in the inset). The same graph is  
656 shown as Fig. 2A of Pastor-Bernier et al. (2020).

657 (D) Histogram of residuals between fitted ICs (with a leave-one-out procedure) and left-out IPs across all participants.  
658 The residuals formed a normal symmetric distribution (red line).

659 (E) Bundle task inside the fMRI scanner. At 4 s after the bundle-on phase, the participant performed in pseudorandomly  
660 selected 50% of trials an additional Becker-DeGroot-Marschak (BDM) task against the computer (bidding 1 - 20 UK  
661 pence). The reward was given if the participant won the BDM (bid  $\geq$  computer bid).

662

### 663 Behavioral validation of indifference curves

664 To assess the contribution and validity of IPs (bundles) to the ICs obtained with hyperbolic fits, we  
665 performed a leave-one-out analysis. The details of these behavioral analyses were presented before

666 (Pastor-Bernier et al. 2020) and are repeated here for completeness. Briefly, we left out (removed)  
 667 one IP at a time from the five IPs within one fitted IC (except for the Reference Bundle at  $x = 0$ ),  
 668 and then we refitted the IC using the remaining four IPs with the same hyperbolic equation (see  
 669 Methods, Eqs. 2, 2a). We performed the same kind of leave-one-IP-out analysis separately for each  
 670 IC in each participant (4 IPs on 3 ICs in 24 participants, resulting in 288 analyses in total).

671 The refitted ICs resulted in consistent fits in four measures. First, there was no overlap in the  
 672 refitted IC with any refitted IC at other levels in all 24 participants; thus, the IC levels retained  
 673 separation despite one IP being left-out. Second, there was no overlap in the 72 refitted ICs with the  
 674 95% confidence intervals of other original ICs at different levels; thus, the IC levels retained  
 675 separation despite one IP being left-out. Third, most refitted ICs (92 %, 66 of 72 ICs) still within the  
 676 95% confidence intervals of the original ICs without the left-out IPs, while the remaining curves  
 677 (8%, 6 of 72 ICs) showed only some parts of the IC that fell outside the 95% confidence intervals;  
 678 thus, individual IPs were not overweighted in the ICs. Fourth, the left-out IPs deviated only  
 679 insignificantly from the refitted ICs ( $P = 0.98$  with t-test;  $N = 336$ ; residual:  $0.05 \pm 0.13$  ml in all  
 680 participants, mean  $\pm$  standard error, SEM) (Fig. 1D); this result confirmed that individual IPs were  
 681 not overweighted in the ICs. These four validations demonstrated the robustness and consistency of  
 682 the hyperbolically fitted ICs in capturing the IPs. Thus, in all participants, the ICs provided valid  
 683 representations of the three revealed preference levels.  
 684

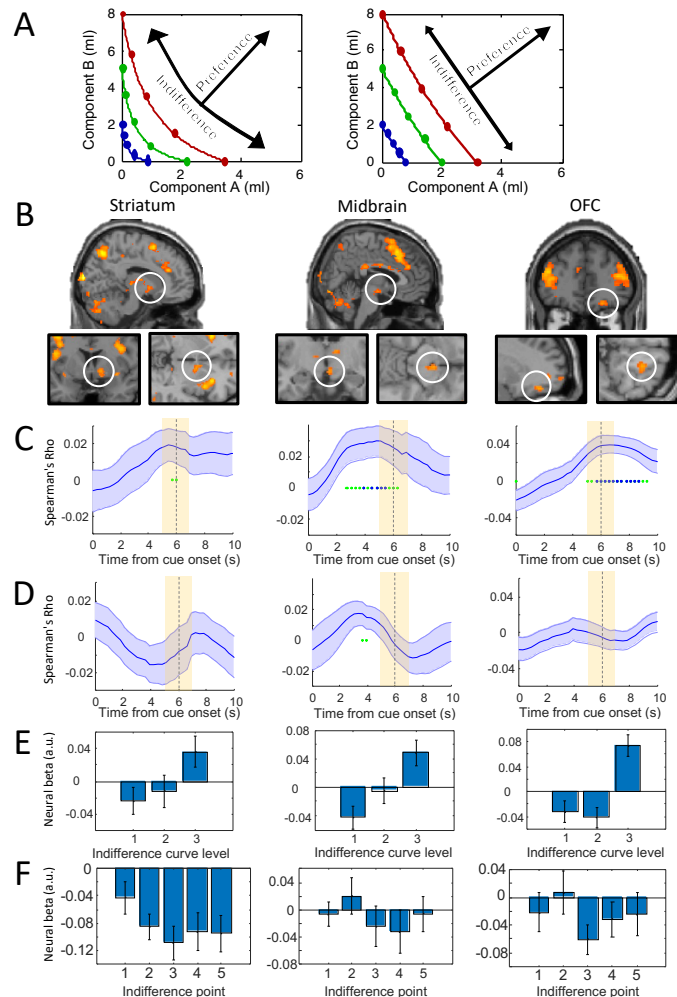
### 685 **Neural responses for two-component bundles across and along ICs**

686 During fMRI scanning, the task started with a fixation cross lasting 0.5 s (Fig. 1E). Then, a single  
 687 two-component visual stimulus appeared in the center of the computer monitor (bundle-on phase);  
 688 the stimulus predicted delivery of one of the 15 bundles (IPs) composed of two different  
 689 milkshakes. The physical amount of the milkshakes in the bundle was determined by the  
 690 participant-specific indifference point (IP) estimated from the binary choice task (see above). The  
 691 participant received the two bundle milkshakes with the respective amounts indicated by the  
 692 vertical bars on the stimulus, without choice. That presentation was either followed by a Becker-  
 693 DeGroot-Marschak (BDM) task within the trial (50% of trials, pseudorandomly selected) or  
 694 terminated (50% of trials). The BDM bidding served as a mechanism-independent measure of  
 695 utility estimation, as used before (de Berker et al. 2019; De Martino et al. 2013). In total, each  
 696 participant performed 360 trials (24 trials for each of the 15 bundles). With the fMRI data we  
 697 collected, we analyzed the various aspects of neural responses (BOLD signals) to the bundles with  
 698 several General Linear Models (GLMs) and region-of-interest (ROI) analyses.

699 We first used GLM1 to identify brain responses that follow the scheme of ICs, namely  
 700 monotonic increase with higher ICs (or decrease with inverse coding) and insignificant change  
 701 along the same ICs, as shown in Fig. 2A. Thus, would BOLD signals change monotonically with  
 702 preference and utility across ICs but vary insignificantly with choice indifference and same utility  
 703 along ICs? To do so, the individual contrast images (representation of BOLD signal) of each bundle  
 704 in each participant were grouped according to the IC the bundle belonged to (low, medium, high)  
 705 and the position of the bundle on each IC (1 - 5, from top left to bottom right).

706 We used parametric statistical tests (t-test with Flexible Factorial Design) and estimated  
 707 neuroimages of responses to each of the 15 bundles grouped into the three IC levels or five groups  
 708 along ICs (see Methods). We found that the striatum, midbrain and OFC showed significantly  
 709 increasing activation across increasing ICs (high > low IC; map threshold of  $p < 0.005$ ; t-test) but  
 710 insignificant variations along individual ICs (exclusive mask map threshold of  $p < 0.005$ ) (Fig. 2B;  
 711 Table 1; for effect sizes, see Table 1-1). More specifically, we found small-volume corrected  
 712 significance in the striatum (peak at [10, 6, -4], z-score = 3.27, 6 mm radius sphere, cluster-level  
 713 FWE corrected  $p = 0.041$ ), midbrain (peak at [4, -16, -12], z-score=3.71, 6 mm radius sphere,  
 714 cluster-level FWE corrected  $p = 0.048$ ) and OFC (peak at [22, 42, -16], z-score = 3.67, 10 mm  
 715 radius sphere, cluster-level FWE corrected  $p = 0.037$ ). (All small-volume corrections in this study  
 716 were centered on pre-defined coordinates from the Neurosynth meta-analysis database, see  
 717 Methods). In addition, we found significant activities in other regions, including the insula and

718 cingulate cortex (Table 1). By contrast, we found significant BOLD changes between bundles  
 719 positioned on same ICs in a number of other, mostly cortical regions (Table 1-2). These changes  
 720 violated the IC scheme representing the trade-off between the two bundle rewards and were not  
 721 further explored.  
 722



723  
 724

725 **Figure 2.** BOLD responses following the revealed preference scheme of two-dimensional indifference curves (ICs).  
 726 (A) Schematic of the analysis method used in GLM1 (arrows): significant BOLD signal across ICs (increasing utility)  
 727 but not within ICs (same utility despite different bundle composition, as inferred from choice indifference). Participants  
 728 typically showed convex ICs (left) or linear ICs (right).

729 (B) BOLD responses discriminating bundles between ICs (map threshold  $p < 0.005$ , extent threshold  $\geq 10$  voxels), but  
 730 no discrimination between bundles along same ICs (map threshold  $p > 0.005$ ; i.e. exclusive mask for brain response  
 731 falls along the same ICs with threshold  $p=0.005$ ) in a group analysis. For activations identified with F contrast, see Fig.  
 732 2-1. For activations identified with the lower threshold of  $p < 0.001$ , see Fig. 2-2.

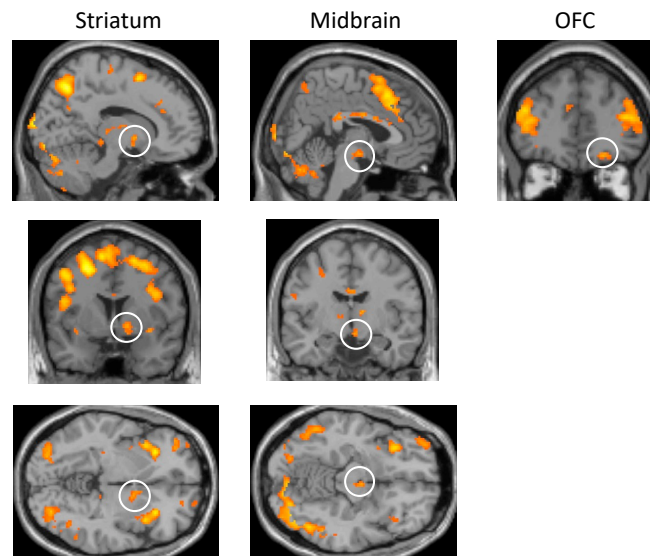
733 (C) Across-IC Spearman rank analyses of brain activations. The Rho coefficients followed the haemodynamic response  
 734 function (HRF) across the 3 IC levels in the ROIs of the three brain structures shown above in B. Solid blue lines  
 735 represent mean Rho from 24 participants;  $\pm$  SEM. Yellow shaded boxes show analysis time window. Green asterisks  $p <$   
 736  $0.05$ , blue asterisks  $p < 0.01$  for t-test of Spearman's Rho against zero. The BOLD responses (input of the Spearman  
 737 rank analyses; with motion parameters regressed out) were extracted from the peak voxels of each participant using  
 738 with a leave-one-out procedure (see Methods).

739 (D) Along-IC ROI activations. The Spearman rank analyses indicated hardly any significance along same ICs in ROIs  
 740 of the three brain structures shown in B.

741 (E) Bar charts of neural beta coefficients of GLM1 for the three IC levels in the three brain structures shown in B in 24  
 742 participants. Bars show mean  $\pm$  SEM.



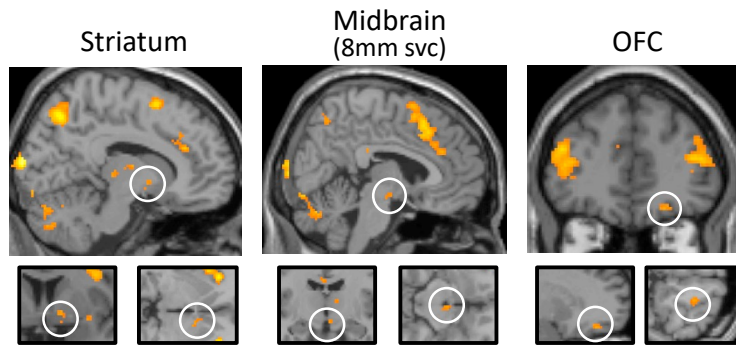
743 (F) Bar charts of neural beta coefficients of GLM1 for all five indifference points (IPs) on same IC levels (neural beta  
 744 coefficients were averaged across the three IC levels in each participant) in 24 participants. Insignificant differences in  
 745 one-way Anova: striatum:  $p = 0.3845$ ,  $F(4,115) = 1.05$ , midbrain:  $p = 0.6828$ ,  $F(4,115) = 0.57$ ; OFC:  $p = 0.5672$ ,  
 746  $F(4,115) = 0.74$ .



747  
 748  
 749 **Figure 2-1.** BOLD responses discriminating bundles between indifference curves (ICs) identified with F contrast (map  
 750 threshold  $p < 0.005$ , extent threshold  $\geq 10$  voxels, high>low), but no discrimination between bundles along same ICs  
 751 (map threshold  $p > 0.005$ ; i.e. exclusive mask for brain response to bundles on same ICs with threshold  $p=0.005$ ) in a  
 752 group analysis. OFC: orbitofrontal cortex.

753  
 754 To provide further evidence for neural activations following the scheme of ICs, we performed  
 755 a Spearman rank time course analysis. We first extracted BOLD signals using leave-one-subject-out  
 756 cross-validated GLM models, which should prevent potential biases with pre-selected peaks (see  
 757 Methods). Subsequently we used the BOLD signals from peak voxels in each left-out subject to  
 758 perform Spearman rank analyses. We found that the striatum, midbrain and OFC showed significant  
 759 Spearman rank correlation coefficients (Spearman's Rho) between bundles located on different ICs  
 760 at around 6s after onset of the bundle stimulus ( $p < 0.05$ ), consistent with the standard time course  
 761 of haemodynamic response (Fig. 2C). By contrast, only insignificant ( $p > 0.05$ ) rank coefficients  
 762 were found at 5 - 7s between bundles located along same ICs in these brain regions, as shown in the  
 763 sliding-window analysis (Fig. 2D). These time courses followed the revealed preference to bundles  
 764 across different ICs but failed to differ along the same IC, thus complying with the scheme of ICs  
 765 that represent revealed preference. Moreover, we extracted beta (slope) coefficients of the BOLD  
 766 signal at 6s with the ROI coordinates identified by GLM1 and plotted them for three revealed  
 767 preference levels in bar charts (Fig. 2E). We found a significant difference between high versus low  
 768 revealed preference level in the midbrain ( $p = 0.0062$ ), OFC ( $p = 0.0023$ ), and marginal significant  
 769 difference in the striatum ( $p = 0.0533$ ). We also found a significant difference between high versus  
 770 middle revealed preference level in the OFC ( $p = 6.8551 \times 10^{-4}$ ). By contrast, a one-way ANOVA  
 771 analysis on the beta (slope) coefficients of the BOLD signal indicated insignificant differences  
 772 between responses to 5 IPs positioned on same ICs in striatum, midbrain and OFC (Fig. 2F). We  
 773 used F contrasts as the exclusive mask and found small volume corrected significance in striatum ( $p$   
 774  $= 0.041$ , 6 mm radius sphere) and OFC ( $p = 0.037$ , 10 mm radius sphere) but only marginal  
 775 significance in midbrain ( $p = 0.051$ , 6 mm radius sphere) (Fig. 2-1). These activations were also  
 776 confirmed with the lower threshold of  $p < 0.001$  (Fig. 2-2; T contrast), with small volume corrected  
 777 significance in striatum ( $p = 0.017$ , 6 mm radius sphere), OFC ( $p = 0.018$ , 10 mm radius sphere) and  
 778 midbrain ( $p = 0.042$ , 8 mm radius sphere; no significance with 6 mm).

779 Taken together, these data indicate that activations in several components of the brain's  
 780 reward system followed the basic scheme of ICs representing revealed preferences: activation  
 781 across the ICs but no activation along the same IC.  
 782

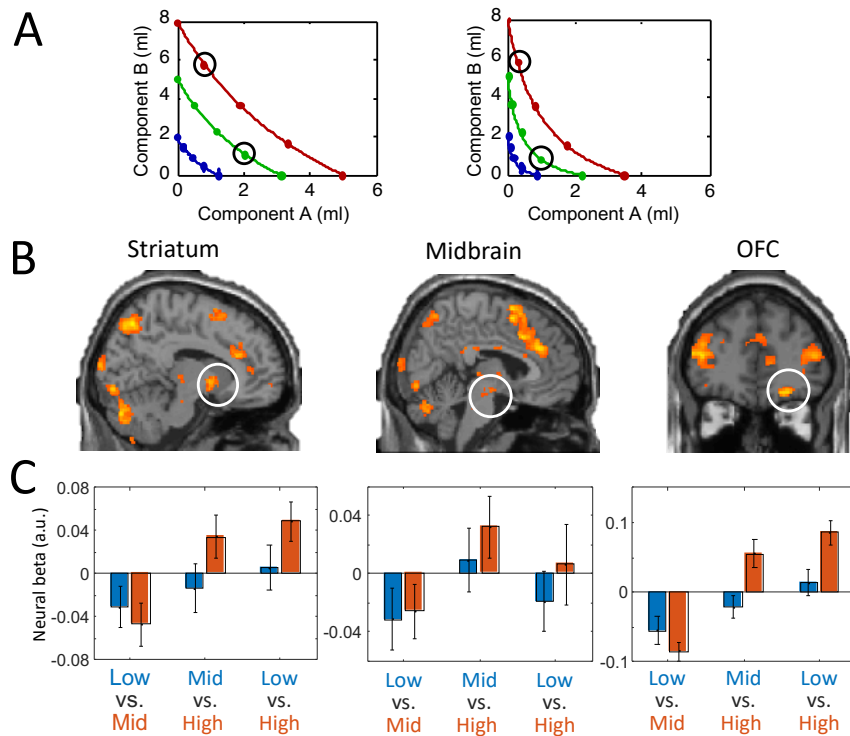


783  
 784  
 785 **Figure 2-2.** BOLD responses discriminating bundles between ICs with lower threshold (map threshold  $p < 0.001$ , extent  
 786 threshold  $\geq 10$  voxels, high  $>$  low), but no discrimination between bundles along same ICs with T contrast (map  
 787 threshold  $p > 0.005$ ; i.e. exclusive mask for brain response to bundles on same ICs with threshold  $p=0.005$ ) in a group  
 788 analysis. Svc: small volume corrected.

### 789 **Binary comparisons between partial physically non-dominant bundles**

790 According to the concept of ICs, any bundle on a higher IC (farther from the origin) should be  
 791 preferred to any bundle on a lower IC. Hence, a single-dimensional neural signal reflecting multi-  
 792 component choice options should vary between any bundle on a higher IC and any bundle on a  
 793 lower IC. To reflect the proper integration of the two bundle components irrespective of specific  
 794 physical properties, the neural signal should follow the IC rank even when one component  
 795 milkshake of the higher-IC bundle is lower than in the lower-IC bundle (partial physical non-  
 796 dominance). To identify such differences, we used the GLM2. With pairwise comparisons, GLM2  
 797 should identify higher responses to revealed preferred bundles with partial physical non-dominance.  
 798 Thus, GLM2 compared all bundle pairs that fit the following condition within each participant:  
 799 bundle 1 was located on higher IC but had a lower amount of one component milkshake compared to  
 800 bundle 2 that was located on a lower IC (Fig. 3A).

801 The GLM2 analysis demonstrated significant activations in similar regions as with GLM1,  
 802 where striatum (peak at [16, 6, -6], z-score=3.8, 6 mm radius sphere, cluster-level FWE corrected  $p$   
 803 = 0.012), midbrain (peak at [4, -16, -12], z-score=2.85, 6 mm radius sphere, cluster-level FWE  
 804 corrected  $p = 0.032$ ) and OFC (peak at [24, 42, -16], z-score=3.99, 10 mm radius sphere, cluster-  
 805 level FWE corrected  $p = 0.012$ ) showed small-volume corrected significant activations (Fig. 3B).  
 806 These activations were also confirmed with the lower threshold of  $p < 0.001$  (Fig. 3-1), with small  
 807 volume corrected significance in striatum ( $p=0.008$ , 6 mm radius sphere) and OFC ( $p=0.004$ , 10  
 808 mm radius sphere). Also, we found significant activities in other regions, including insula, superior  
 809 frontal gyrus and cingulate, as shown in Table 2.  
 810

811  
812813  
814815  
816817  
818819  
820821  
822823  
824825  
826827  
828829  
830831  
832833  
834835  
836837  
838839  
840841  
842

**Figure 3.** Higher BOLD responses to more preferred (but physically partially dominated) bundles positioned on different indifference curves (ICs).

(A) Two examples of binary bundle comparison. Each pair of black circles indicates one binary comparison in one participant.

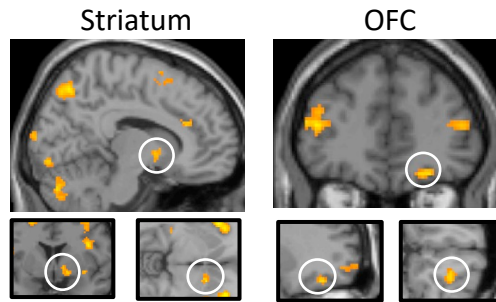
(B) Brain regions activated more by preferred bundles compared to alternative bundles in group analysis with GLM2. Map threshold  $p < 0.005$ , extent threshold  $\geq 10$  voxels. For activations identified with the lower threshold of  $p < 0.001$ , see Fig. 3-1.

(C) Bar charts showing neural beta coefficients of regression in ROIs of three brain structures in the population of 24 participants. Each group of bars (3 groups in each ROI) shows the beta coefficients for bundles in partial physically dominating relationships on different ICs: low vs. mid; mid vs. high and low vs. high. Orange bars represent the higher preference level and blue bars represent the lower preference level in each comparison. The bars show the mean  $\pm$  SEM. For activations at peak voxels, see Fig. 3-2.

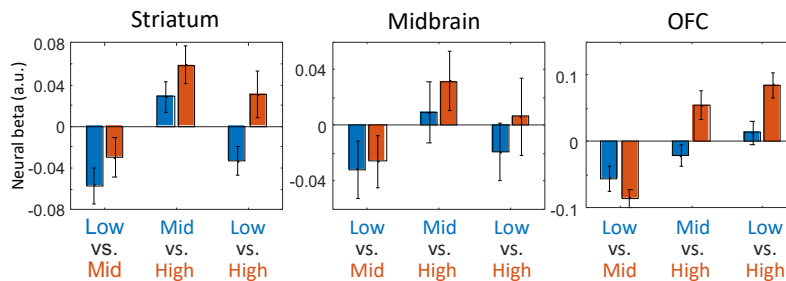
We also performed ROI analyses (coordinates identified by GLM2 with leave-one-subject-out procedure) that calculated betas of partial physical non-dominance (higher revealed preference) and partial physical dominance bundles (lower revealed preference) as described in Methods. For each ROI, we computed three models, which compared bundles pairwise, with low vs. middle, middle vs. high, and low vs. high revealed preference, respectively. Neural beta regression coefficients were extracted at 6 s after the onset of the bundle stimulus, which corresponded to the canonical hemodynamic response. In regard to high vs. low revealed preference level, we found significance in the striatum ( $p = 0.0459$ ) and OFC ( $p = 0.0033$ ) when comparing bundles in high IC vs. low IC (Fig. 3C). We also found significance in the striatum ( $p = 0.0309$ ) and OFC ( $p = 7.6575 \times 10^{-5}$ ) when comparing high vs. middle IC bundles. In the midbrain, we found no significance ( $p > 0.05$ ) in the three comparisons between bundles on low, middle and high ICs (although such a tendency existed in all three comparisons). When plotting Figure 3C using peak voxels from GLM1, we found similar results for all three regions (Fig. 3-2), which is unsurprising as the coordinates were similar between GLM1 and GLM2. Thus, the region-of-interest analysis was robust with GLM1 coordinates for these regions.

Taken together, these pairwise bundle comparisons demonstrated neural coding of partial physical non-dominance bundles as a necessary condition for extracting a scalar neural signal from

843 vectorial, multi-component choice options. These results confirmed compliance with the graphic  
 844 schemes of ICs demonstrated with GLM1.  
 845



846  
 847  
 848 **Figure 3-1.** Higher BOLD responses to more preferred (but physically partially dominated) bundles positioned on  
 849 different indifference curves with stricter thresholds (Map threshold  $p < 0.001$ , extent threshold  $\geq 10$  voxels) in striatum  
 850 (left) and OFC (right).  
 851



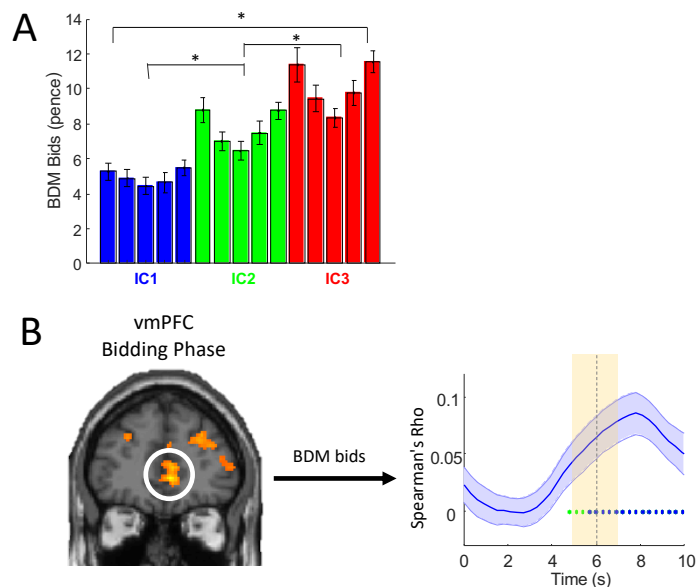
852  
 853  
 854 **Figure 3-2.** Bar charts showing neural beta coefficients of regression at peak voxels in ROIs (with ROIs coordinate  
 855 extracted from GLM1 using leave-one-out procedure) of three brain structures in the population of 24 participants. Each  
 856 group of bars (3 groups in each ROI) shows the beta coefficients for bundles in partial physically dominating  
 857 relationships on different indifference curves (IC): low vs. mid; mid vs. high and low vs. high. Orange bars represent  
 858 the higher preference level and blue bars represent the lower preference level. The bars show the mean  $\pm$  SEM.  
 859

### 860 **Becker-DeGroot-Marschak (BDM) control of revealed preference**

861 To validate the order of revealed preferences represented by the ICs with an independent estimation  
 862 mechanism, we used a monetary Becker-DeGroot-Marschak (BDM) bidding task that estimated  
 863 each participant's utility for each bundle. In 50% of trials during fMRI scanning, each participant  
 864 made a monetary BDM bid (UK pence) for one of the 15 bundles, out of a fresh endowment of 20  
 865 UK pence in each trial (BDM bidding phase; Fig. 1E). The 15 bundles constituted the indifference  
 866 points of the ICs that were estimated during the binary choice task with each participant.

867 The BDM bids followed the order of revealed preference levels across ICs, as demonstrated  
 868 by significant positive Spearman Rank correlation between the three IC levels and the bid amounts  
 869 for bundles and confirmed with significant binary Wilcoxon signed-rank tests between the three IC  
 870 levels (Fig. 4A; blue, green, red). By contrast, there was no correlation between bids for the five  
 871 bundles and their position along each IC (from top left to bottom right; Spearman Rho = 0.0219;  $p =$   
 872 0.6791). Thus, BDM bids increased across the three IC levels but did not change monotonically  
 873 with bundle position along individual ICs in the population of our participants.

874 In order to investigate neural mechanisms of BDM bidding and value elicitation, we  
 875 compared two GLM models: (1) GLM3 to identify brain regions that encoded BDM bids (0 - 20  
 876 pence) during the bidding phase, as shown in Fig. 4B; (2) GLM1 to identify brain regions that  
 877 encoded value elicitation according to IC levels during bundle-on phase, as shown above in Fig. 2B,  
 878 C, far right.



879  
880  
881  
882  
883  
884  
885  
886  
887  
888  
889

**Figure 4.** Activation in ventromedial prefrontal cortex (vmPFC) during BDM bidding.

(A) Bar chart for BDM bids for 15 bundles of 24 participants (mean  $\pm$  SEM). The colors of the bars indicate the indifference curves (IC) to which the bundle belongs (blue = low IC; green = middle IC; red = high IC). Spearman rank correlation: across ICs:  $Rho = 0.5710$ ,  $p = 1.5659 \times 10^{-32}$ ; within IC:  $Rho = 0.0219$ ,  $p = 0.6791$ . Wilcoxon signed rank test: IC1 vs. IC2:  $p = 1.2802 \times 10^{-20}$ ; IC2 vs. IC3:  $p = 8.0748 \times 10^{-21}$ ; IC1 vs. IC3:  $p = 1.5954 \times 10^{-19}$ .

(B) vmPFC activation during bidding phase (GLM3: activation correlated with BDM bids; threshold  $p < 0.005$ , extent threshold  $\geq 10$  voxels). Spearman rank analysis (right) showed significant Rho coefficient across bids. For additional activation in dorsal striatum, see Fig. 4-1.

890  
891  
892  
893  
894  
895  
896  
897  
898  
899  
900  
901  
902

Analysis with GLM3 demonstrated activation in vmPFC that encoded BDM bids during the bidding phase (Fig. 4B left; peak at [6, 44, 0],  $z$ -score = 4.10, whole-brain corrected with cluster-level FWE corrected  $p = 0.002$ ), together with other brain regions (Table 3). Further ROI analysis showed significant rank correlation between vmPFC activation and BDM bids at around 6 s after BDM cue onset (Fig. 4B right; bidding phase;  $p < 0.05$ ; Spearman's Rho), consistent with the expected haemodynamic response function. By contrast, analysis with GLM1 showed significant, small-volume corrected activation in OFC that indicated its involvement in encoding IC levels during the bundle-on phase (Fig. 2B; far right). The ROI analysis showed significant rank correlation between OFC activation and IC levels at around 6 s after bundle onset (Fig. 2C; far right; bundle-on phase;  $p < 0.05$ ; Spearman's Rho). In addition, with GLM3, we found small-volume corrected significant activation in the dorsal striatum (Fig. 4-1; peak at [12, 12, 0],  $z$ -score = 3.53, 6 mm radius sphere, cluster-level FWE corrected  $p = 0.008$ ) encoding the BDM bids but not in the ventral striatum ( $p > 0.1$ ).

903  
904  
905  
906

Taken together, BDM bidding provided a good validation of the estimated levels of revealed preference represented by ICs. However, and interestingly, revealed preference levels and BDM bids were encoded in different regions of the frontal cortex and striatum.



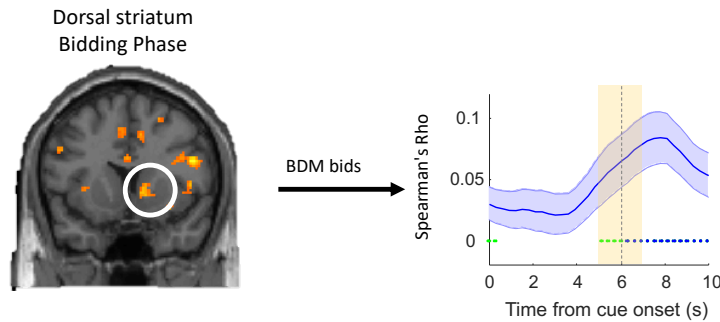


**Figure 4-1.** Dorsal striatum activation during bidding phase (GLM3: activation correlated with the amount of BDM bids; threshold  $p < 0.005$ , extent threshold  $\geq 10$  voxels). Brain map (left) shows dorsal striatum activity during bidding phase. Spearman rank analysis (right) showed significant Rho coefficient across bids during bidding phase in dorsal striatum.

## Discussion

We systematically tested characteristics of scalar neural responses to vectorial, multi-component bundles. We estimated indifference points (IPs) by asking human participants to choose between two bundles. Each bundle contained the same two separate objects (milkshakes) rather than consisting of single objects that each had multiple components. Our behavioral results (Pastor-Bernier et al. 2020) showed that preference relationships among multi-component choices were reliably represented by systematic ICs, as a prerequisite for testing the underlying neural mechanisms. In fMRI scans with GLM and post-hoc ROI analyses, we identified brain regions whose activations correlated with levels of revealed preference. The GLM1 and post-hoc Spearman rank analysis demonstrated activations in the ventral striatum, midbrain and OFC that reflected revealed preference levels across ICs (changing utility) but failed to vary along equal-preference ICs (same utility despite different bundle composition). The GLM2 specifically dissociated revealed preference from physical dominance and showed consistent results with those from GLM1. A mechanism-independent control with a Becker-DeGroot-Marschak (BDM) bidding task confirmed the validity of ICs for representing revealed preference levels. Interestingly, however, BDM bidding was associated with activations in vmPFC and dorsal striatum rather than the previously identified reward structures following IC levels. Together, these data demonstrate systematic, single-dimensional neural activations in the striatum, midbrain and OFC that reflect preferences for, and utility of, vectorial multi-component choice options.

Scalar neural activations from vectorial choice options are only the most simple way to represent value integrated from multiple components. Other plausible but less straightforward ways might be ensemble coding composed of multiple heterogeneous signals representing only single components of multi-component options, as seen in individual OFC neurons (Pastor-Bernier et al. 2019). Future neuroimaging studies may address such issues.

In our binary choice task, we elicited revealed preferences with repeated, psychophysically controlled choices (Pastor-Bernier et al. 2020; Green, & Swets 1966). Such a multi-trial, stochastic approach is well conceptualized (McFadden & Richter 1990; McFadden 2004), fulfils statistical requirements of neural research, corresponds to standard choice functions (Sutton, & Barto 1998), and allows comparison with animal neurophysiology (Pastor-Bernier et al., 2017). These methods delivered varying choice probabilities (stochastic choices) instead of single selections (deterministic choices).

Economic choice experiments often involve substantial but imaginary sizes or amounts of consumer items and money, or use random singular payouts (Simonson, 1989; Tversky & Simonson 1993; Rieskamp et al., 2006). By contrast, our payout schedule fit the requirements of neuroimaging and involved tangible and consumable rewards over hundreds of trials, while also controlling for

950 satiety. The behavioral choices resembled small daily activities, such as drink and snack  
951 consumption. In this way, we obtained three well-ordered ICs for each participant that provided  
952 accurate and systematic representations of preferences for multi-component bundles, without  
953 involving imagined items or monetary reward (Pastor-Bernier et al. 2020).

954 We used the BDM task as an authoritative, mechanism-independent control for eliciting  
955 subjective values, thereby providing an additional validating mechanism for the revealed  
956 preferences elicited in our binary choice test. The value estimating mechanism for BDM bids differs  
957 substantially from the one for revealed preference ICs. The truthful revelations (incentive  
958 compatibility) of BDM makes this mechanism an essential tool in experimental economics that is  
959 becoming more popular in human decision research (Plassmann et al., 2007; Medic et al., 2014;  
960 Zangemeister et al., 2016). The elicited BDM bids correlated well with the revealed preference  
961 levels (Pastor-Bernier et al., 2020) and thereby validated in a mechanism-independent manner the  
962 empirically estimated IPs used during fMRI (in which the participants performed the BDM task).  
963 Previous neuroimaging studies showed activations in ventromedial prefrontal cortex that correlated  
964 with BDM bids (Chib et al., 2009; McNamee et al., 2013). Our experimental design dissociated  
965 value elicitation by bundles and by BDM bidding. We confirmed the BDM activations in vmPFC  
966 and found that the two mechanistically different tasks activated different regions in both prefrontal  
967 cortex and striatum; responses to the bundles followed the IC scheme (different activations across  
968 but not within ICs) in OFC and ventral striatum, whereas BDM bidding activated vmPFC and  
969 dorsal striatum. Previous studies showed that vmPFC activity can reflect value derived from both  
970 rating measures and can distinguish between preferred and non-preferred options irrespective of  
971 task demands (Lebreton et al., 2009; Lopez-Persem et al., 2020). Thus, the conditions under which  
972 vmPFC encodes value, and the precise form of value-elicitation that best explains vmPFC activity  
973 are valuable topic for future studies..

974 Previous studies tested neural mechanisms of human choice of bundles with multiple  
975 components, such as payoff amount and probability (Chau et al. 2014), quality and quantity of  
976 goods (de Berker et al. 2019), money and time (Gluth et al. 2017), and food components (Suzuki et  
977 al. 2017). Nevertheless, none of these studies tested bundles that were positioned along modelled  
978 ICs (i.e. eliciting choice indifference) and thus failed to test the crucial trade-off that demonstrates  
979 the graded and well-ordered manner of single-dimensional preferences for multi-dimensional choice  
980 options. Without this information, we would not know how a scalar neural response may arise from  
981 graded changes of vectorial, multi-component bundles. Our study, testing 5 bundles on each IC,  
982 addressed this problem and identified the brain regions that showed this kind of neural response.

983 Although we tested the emergence of single-dimensional neural signals for multi-dimensional  
984 bundles in a systematic and concept-driven way, there were limitations with our experimental  
985 design. First, both bundle components had the same type of primary reward (milkshakes). It would  
986 be interesting to study whether the same brain regions would encode different types of rewards and  
987 follow the formalisms of ICs, including the graded trade-off. For instance, future research may  
988 compare monetary rewards with primary nutrient rewards. Second, we only demonstrated neural  
989 responses with the typical convex ICs. It would be interesting to study whether different brain  
990 regions might encode preferences with different shapes of ICs. Such work may test participants'  
991 choices with linear or concave ICs. Third, we did not test the influences of prior experience on  
992 current decisions. Previous studies (Schultz 1998; van den Bos et al. 2013; Lopez-Persem et al.  
993 2016) showed that choices could be influenced by previous experience and be updated by  
994 reinforcement learning. Future research may include multi-component choice options during fMRI  
995 scanning to study multi-component reinforcement learning. Lastly, we only demonstrated fMRI  
996 BOLD responses, and future neurophysiology research should confirm the coding of revealed  
997 preference at a single neuron level in human patients with intracerebrally implanted electrodes,  
998 similar to our recently investigated neuronal encoding of revealed preference in monkey  
999 orbitofrontal cortex (Pastor-Bernier et al. 2019). To conclude, while we showed brain activation  
1000 with bundles in a formal but standard revealed preference setting (convex ICs, primary reward), it is  
1001 desirable to know how human brains encode revealed preference in a larger variety of situations.

1002 The reward circuit including the striatum and midbrain is known to participate in reward  
 1003 anticipation and learning, including reward prediction error (Diederer et al. 2017). In monkeys,  
 1004 midbrain dopamine neurons encode values for predicted rewards in economic decision tasks (Lak et  
 1005 al. 2016; Schultz et al. 2017). Similar to the midbrain and striatum, previous work showed the  
 1006 involvement of the human mid-OFC in valuation of primary nutrient reward (Grabenhorst et al.,  
 1007 2010) and monetary reward (Kahnt et al. 2014). Remarkably, the neural activity in OFC elicited  
 1008 here, in response to visual cues predicting liquid rewards with varying sugar and fat components,  
 1009 closely matched the coordinates observed previously (Grabenhorst et al., 2010) in a study in which  
 1010 subjects orally sampled very similar liquid rewards. Thus, this area of OFC seems to be involved  
 1011 both in reward valuation during oral consumption of primary nutrient rewards and in the economic  
 1012 valuation of visually cued choice options. In non-human primates, OFC neurons encode reward  
 1013 prediction (Tremblay & Schultz 1999; Padoa-Schioppa & Assad 2006) and follow revealed  
 1014 preferences for multi-component bundles (Pastor-Bernier et al. 2019). In the current study, we used  
 1015 a concept-driven design and found that neural responses in the striatum, midbrain and OFC  
 1016 integrated multiple bundle components in a way that followed the ICs scheme (changing across ICs  
 1017 but being similar along equal-preference ICs). Moreover, we demonstrate the involvement of the  
 1018 midbrain in multi-component decision making for the first time. Overall, our results show the  
 1019 involvement of principal reward structures of the brain in integrating the multiple components of  
 1020 vectorial bundles into single-dimensional neural signals that are suitable for economic decision  
 1021 making.

1022 Besides the primary reward circuit (midbrain dopamine neurons, OFC, striatum, amygdala),  
 1023 other brain regions are also involved in economic decision making. Previous studies in multi-  
 1024 component decision making suggested the involvement of the cingulate, prefrontal cortex and  
 1025 insula in value elicitation (Kurtz-David et al. 2019; Busemeyer et al. 2019). Consistent with these  
 1026 studies, we also found significant activation in these regions. As shown in Table 1 and Table 2, the  
 1027 BOLD signals identified by GLM1 and GLM2 showed that these regions also encode bundle values  
 1028 during the bundle-on phase, together with the striatum, midbrain, and mid-OFC. Our results are  
 1029 consistent with these previous studies, suggesting that a considerable number of brain regions also  
 1030 play a role in multi-component decision making.

1031

1032

## 1033 **References**

1034

1035 Amemiya T (1981) Qualitative response models: A survey. *J Econ Litt* 19:1483-1536.

1036 Becker GM, DeGroot MH, Marschak J (1964) Measuring utility by a single-response sequential  
 1037 method. *Behav Sci* 9:226-232.

1038 Busemeyer JR, Gluth S, Rieskamp J, Turner BM (2019) Cognitive and neural bases of multi-  
 1039 attribute, multi-alternative, value-based decisions. *TICS* 23:251-263.

1040 Chau BKH, Kolling N, Hunt LT, Walton ME, Rushworth MFS (2014) A neural mechanism  
 1041 underlying failure of optimal choice with multiple alternatives. *Nat Neurosci* 17:463-470.

1042 Chib VS, Rangel A, Shimojo S, O'Doherty JP (2009) Evidence for a common representation of  
 1043 decision values for dissimilar goods in human ventromedial prefrontal cortex. *J Neurosci*  
 1044 29:12315-12320.

1045 Chung HK, Sjöström T, Lee HJ, Lu YT, Tsuo FY, Chen TS, Chang CF, Juan CH, Kuo WJ, Huang  
 1046 CY (2017) Why do irrelevant alternatives matter? An fMRI-TMS study of context-dependent  
 1047 preferences. *J Neurosci* 37:11647-11661.

1048 de Berker AO, Kurth-Nelson Z, Rutledge RB, Bestmann S, Dolan RJ (2019) Computing value from  
 1049 quality and quantity in human decision-making. *J Neurosci* 39:163-176.

1050 De Martino B, Fleming SM, Garrett N, Dolan RJ (2013) Confidence in value-based choice. *Nat*  
 1051 *Neurosci* 16:105-110.

1052 De Martino B, Kumaran D, Holt B, Dolan RJ (2009) The neurobiology of reference-dependent  
 1053 value computation. *J Neurosci* 29:3833-3842.



- 1054 Diederer KM, Ziauddeen H, Vestergaard MD, Spencer T, Schultz W, Fletcher PC (2017) Dopamine  
 1055 modulates adaptive prediction error coding in the human midbrain and striatum. *J Neurosci*  
 1056 37:1708-1720.
- 1057 Fujiwara J, Tobler PN, Taira M, Iijima T, Tsutsui KI (2009) Segregated and integrated coding of  
 1058 reward and punishment in the cingulate cortex. *J Neurophysiol* 101:3284-3293.
- 1059 Gluth S, Hotaling JM, Rieskamp J (2017) The attraction effect modulates reward prediction errors  
 1060 and intertemporal choices. *J Neurosci* 37: 71-382.
- 1061 Grabenhorst F, Rolls ET, Parris BA, D'Souza A (2010) How the brain represents the reward value  
 1062 of fat in the mouth. *Cereb Cortex* 20:1082-1091.
- 1063 Green DM, Swets J. (1966) *Signal detection theory and psychophysics*: New York: Wiley.
- 1064 Hunt LT, Dolan RJ, Behrens TE (2014) Hierarchical competitions subserving multi-attribute choice.  
 1065 *Nat Neurosci* 17:1613-1620.
- 1066 Kagel JH, Battalio RC, Rachlin H, Basmann RL, Green L, Klemm WR (1975) Experimental studies  
 1067 of consumer demand behavior using laboratory animals. *Econ Inquiry* 13:22-38.
- 1068 Kahnt T, Park SQ, Haynes JD, Tobler PN (2014) Disentangling neural representations of value and  
 1069 salience in the human brain. *Proc Nat Acad Sci* 111:5000-5005.
- 1070 Knetsch JL (1989) The endowment effect and evidence of nonreversible indifference curves. *Am*  
 1071 *Econ Rev* 79:1277-1288.
- 1072 Kurtz-David V, Persitz D, Webb R, Levy DJ (2019) The neural computation of inconsistent choice  
 1073 behavior. *Nat Comm* 10:1583.
- 1074 Lak A, Stauffer WR, Schultz W. (2016) Dopamine neurons learn relative chosen value from  
 1075 probabilistic rewards. *eLife* 5:e18044.
- 1076 Lebreton M, Jorge S, Michel V, Thirion B, Pessiglione M (2009) An automatic valuation system in  
 1077 the human brain: evidence from functional neuroimaging. *Neuron* 64:431-439.
- 1078 Lopez-Persem A, Bastin J, Petton M, Abitbol R, Lehongre K, Adam C, Navarro V, Rheims S,  
 1079 Kahane P, Domenech P, Pessiglione M (2020) Four core properties of the human brain  
 1080 valuation system demonstrated in intracranial signals. *Nat Neurosci* 23:64-675.
- 1081 Lopez-Persem A, Domenech P, Pessiglione M (2016) How prior preferences determine decision-  
 1082 making frames and biases in the human brain. *Elife* 5:e20317.
- 1083 Mas-Colell A, Whinston MD, Green JR (1995) *Microeconomic theory*. New York: Oxford Univ  
 1084 Press.
- 1085 McFadden D, Richter MK (1990) Stochastic rationality and revealed stochastic preference. In:  
 1086 *Preferences, Uncertainty, and Optimality. Essays in Honor of Leo Hurwicz*, Westview Press:  
 1087 Boulder, CO, 161-186.
- 1088 McFadden DL (2004) Revealed stochastic preference: A synthesis. *Econ Theory* 26:245-264.
- 1089 McNamee D, Rangel A, O'Doherty JP (2013) Category-dependent and category-independent goal-  
 1090 value codes in human ventromedial prefrontal cortex. *Nat Neurosci* 16:479-485.
- 1091 Medic N, Ziauddeen H, Vestergaard MD, Henning E, Schultz W, Farooqi IS, Fletcher PC (2014)  
 1092 Dopamine modulates the neural representation of subjective value of food in hungry subjects. *J*  
 1093 *Neurosci* 34:16856-16864.
- 1094 Padoa-Schioppa C, Assad JA (2006) Neurons in the orbitofrontal cortex encode economic value.  
 1095 *Nature* 441:223-226.
- 1096 Pastor-Bernier A, Plott CR, Schultz W (2017) Monkeys choose as if maximizing utility compatible  
 1097 with basic principles of revealed preference theory. *Proc Nat Acad Sci* 114:E1766-E1775.
- 1098 Pastor-Bernier A, Stasiak A, Schultz W (2019) Orbitofrontal signals for two-component choice  
 1099 options comply with indifference curves of Revealed Preference Theory. *Nature Comm* 10:1-  
 1100 19.
- 1101 Pastor-Bernier A, Volkmann K, Stasiak A, Grabenhorst F, Schultz W (2020) Experimentally  
 1102 revealed stochastic preferences for multi-component choice options. *J exp Psychol: Anim*  
 1103 *Learn Cog* (in press).
- 1104 Plassmann H, O'Doherty J, Rangel A (2007) Orbitofrontal cortex encodes willingness to pay in  
 1105 everyday economic transactions. *J Neurosci* 27:9984-9988.

- 1106 Razzaghi M (2013) The Probit Link Function in Generalized Linear Models for Data Mining  
1107 Applications. *J Mod Appl Stat Meth* 12:Article 19.
- 1108 Rieskamp J, Busemeyer JR, Mellers BA (2006) Extending the bounds of rationality: Evidence and  
1109 theories of preferential choice. *J Econ Lit* 44:631-661.
- 1110 Samuelson PA, (1938) A note on the pure theory of consumer's behavior. *Economica* 5:61-71.
- 1111 Schultz W (1998) Predictive reward signal of dopamine neurons. *J Neurophysiol* 80:1-27.
- 1112 Schultz W, Stauffer WR, Lak A (2017) The phasic dopamine signal maturing: from reward via  
1113 behavioural activation to formal economic utility. *Curr Op Neurobiol* 43:139-148.
- 1114 Simonson I (1989) Choice based on reasons: The case of attraction and compromise effects. *J*  
1115 *Consum Res* 16:158-174.
- 1116 Sutton RS, Barto AG (1998) Reinforcement Learning: An Introduction. Cambridge MA: MIT Press.
- 1117 Suzuki S, Cross L, O'Doherty JP (2017). Elucidating the underlying components of food valuation  
1118 in the human orbitofrontal cortex. *Nat Neurosci* 20:1780-1786.
- 1119 Tremblay L, Schultz W (1999) Relative reward preference in primate orbitofrontal cortex. *Nature*  
1120 398:704-708.
- 1121 Tversky A, Simonson I (1993) Context-dependent preferences. *Management Sci* 39:1179-1189.
- 1122 van den Bos W, Talwar A, McClure SM (2013) Neural correlates of reinforcement learning and  
1123 social preferences in competitive bidding. *J Neurosci* 33:2137-2146.
- 1124 Yamagata N, Ichinose T, Aso Y, Plaçais PY, Friedrich AB, Sima RJ, Preat T, Rubin GM, Tanimoto  
1125 H. (2015) Distinct dopamine neurons mediate reward signals for short-and long-term  
1126 memories. *Proc Nat Acad Sci* 112: 78-583.
- 1127 Yarkoni T, Poldrack RA, Nichols TE, Van Essen DC, Wager TD (2011) Large-scale automated  
1128 synthesis of human functional neuroimaging data. *Nat Meth*:665-670.
- 1129 Zangemeister L, Grabenhorst F, Schultz W (2016) Neural basis for economic saving strategies in  
1130 human amygdala-prefrontal reward circuits. *Curr Biol* 26:3004-3013.
- 1131

1132  
1133  
1134  
1135

**Table 1.** Brain regions activated across but not along indifference curves (ICs) during bundle-on phase (whole-brain analysis with GLM1).

Brain region	Hemisphere	MNI peak coordinates (x,y,z)	peak z-score
Striatum*	R	10, 6, -4	3.27
Midbrain*	/	4, -16, -12	3.09
OFC*	R	22, 42, -16	3.67
Parieto-occipital transition zone/ occipital gyri	/	-12, -66, 46	7.42
Insular gyrus/ basal operculum	L	-30, 18, 2	5.80
	R	32, 26, -4	4.91
Superior frontal gyrus	/	-24, 2, 52	5.70
Middle frontal gyrus	L	-42, 2, 42	4.98
		-40, 34, 18	4.74
	R	44, 46, 16	4.94
Cingulate gyrus	/	-2, -24, 28	4.87
Precentral gyrus	R	40, 6, 24	4.59
Angular gyrus	L	-22, -72, 54	3.89

1136  
1137  
1138  
1139  
1140  
1141  
1142  
1143  
1144

Cluster P values ( $P < 0.05$ ) with family-wise error correction across the whole brain. Map threshold  $P < 0.005$  (across ICs; high>low IC) with exclusive contrast map  $P > 0.005$  (along ICs), extent threshold  $\geq 10$  voxels. \* $P < 0.05$  with small volume correction correction (6mm radius for striatum and midbrain; 10mm for OFC) using coordinates from Neurosynth meta-analysis database (see Methods). '/' indicates activation close to and crossing the midline. For effect sizes, see Table 1-1. For significant BOLD changes between bundles positioned on same ICs in other brain regions, see Table 1-2.

1145  
1146  
1147  
1148

**Table 1-1.** Effect sizes for BOLD responses to bundles positioned across and along indifference curves (IC) in striatum, midbrain and OFC (GLM1).

Brain region	Preference (different utility)	Choice indifference (same utility)	
	Effect across ICs	Effect along ICs (T statistics)	Effect along ICs (F statistics)
Striatum	Z = 3.27 p = 0.041	N/A (Fat) N/A (Sugar)	N/A
Midbrain	Z = 3.09 p = 0.048	N/A (Fat) N/A (Sugar)	N/A
OFC	Z = 3.67 p = 0.037	Z = 2.77, p = 0.188 (Fat) N/A (Sugar)	N/A

1149  
1150  
1151  
1152  
1153  
1154

P values refer to small volume corrected BOLD signal (6mm radius for striatum and midbrain; 10mm for OFC) using coordinates from Neurosynth (see Methods). Map threshold  $P < 0.005$ , extent threshold  $\geq 10$  voxels. Z: peak z-score. Threshold  $p = 0.005$  with extent threshold  $\geq 10$  voxels, tested with small volume correction. N/A: no cluster of voxels met the statistical criteria.

1155  
1156  
1157  
1158

**Table 1-2.** Brain regions activated along indifference curves (ICs) during bundle-on phase (whole-brain analysis with GLM1 F contrast along ICs).

Brain region	Hemisphere	MNI peak coordinates (x,y,z)	peak z-score
Striate area	/	2, -86, 6	>8
Inferior frontal gyrus, orbital part/ Lateral OFC	R	46, 50, -2	4.63
Inferior frontal gyrus, triangular part	R	56, 16, 0	4.14
Middle temporal gyrus	R	64, -24, -18	4.41
Superior frontal gyrus, medial part	/	4, 38, 26	4.37
Supramarginal gyrus	R	48, -50, 42	4.31
Inferior temporal gyrus	L	-32, -78, -16	3.86
Superior temporal gyrus	L	-56, -46, 40	3.74

1159  
1160  
1161  
1162  
1163

Cluster P values ( $P < 0.05$ ) with family-wise error correction across the whole brain. Map threshold  $P < 0.005$  (along ICs), extent threshold  $\geq 10$  voxels. '/' indicates activation close to and crossing the midline.

1164  
1165  
1166  
1167  
1168

**Table 2.** Brain regions showing differences (partial physical non-dominance > partial physical dominance) in BOLD signal between partial physically dominating bundles located on different indifference curves (ICs) during bundle-on phase (whole-brain analysis with GLM2).

Brain region	Hemisphere	MNI peak coordinates (x,y,z)	peak z-score
Striatum*	R	16, 6, -6	3.8
Midbrain*	/	4, -16, -12	2.85
OFC*	R	24, 42, -16	3.99
Insular gyrus/ Basal operculum	L	-30, 24, -2	5.55
	R	32, 26, -6	4.40
Angular gyrus	R	32, -68, 28	5.51
Cerebellum	L	-36, -68, -30	4.79
Superior frontal gyrus	/	22, 2, 54	4.75
Occipital gyri	L	-28, -88, 4	4.57
Middle frontal gyrus	L	-50, 40, 16	4.32
	R	46, 42, 14	3.76
Inferior frontopolar gyrus	R	18, 64, -8	4.11
Cingulate gyrus	/	-2, -24, 28	4.05

1169  
1170  
1171  
1172  
1173  
1174

Cluster P values ( $P < 0.05$ ) with family-wise error correction across the whole brain. Map threshold  $P < 0.005$ , extent threshold  $\geq 10$  voxels. \* $P < 0.05$  with small volume correction (6mm radius for striatum and midbrain; 10mm for OFC) using coordinates from Neurosynth meta-analysis database (see Methods).

1175  
1176  
1177  
1178

**Table 3.** Brain regions with BOLD responses correlating with BDM bids during the bidding phase (whole-brain analysis with GLM3).

Brain region	Hemisphere	MNI peak coordinates (x,y,z)	peak z-score
vmPFC	/	6, 44, 0	4.10
Dorsal striatum*	R	12, 12, 0	3.53
Insular gyrus/ basal operculum	R	30, 24, -2	5.21
Inferior frontal gyrus, opercular part	R	46, 8, 22	4.76
Occipital gyri	L	-36, -90, -2	4.67
Superior parietal lobule	L	-30, -56, 46	4.14
Superior frontal gyrus	/	2, 26, 42	4.05
Middle frontal gyrus	R	38, 36, 18	3.93
Postcentral gyrus	R	32, -36, 48	3.62
Inferior frontopolar gyrus	R	22, 56, -4	3.53

1179  
1180  
1181  
1182  
1183

Cluster P values ( $P < 0.05$ ) with family-wise error correction across the whole brain. Map threshold  $P < 0.005$ , extent threshold  $\geq 10$  voxels. \* $P < 0.05$  with small volume correction (6 mm radius) using coordinates from a previous study with BDM bidding (De Martino et al., 2009; see Methods).